

Atomic and Molecular Layer Deposition of Functional Thin Films Based on Rare Earth Elements

Amr Ghazy, David Zanders, Anjana Devi,* and Maarit Karppinen*

High-quality rare earth element (R) based thin films are in demand for applications ranging from (optoelectronics and energy conversion/storage to medical diagnostics, imaging and security technologies. Atomic layer deposition (ALD) offers large-area homogeneous and conformal ultrathin films and is uniquely suited to address the requirements set by the potential applications of R-based thin films. The history starts from the 1990s, when the first electroluminescent R-doped thin films were grown with ALD. The interest soon expanded to rare earth element oxide layers as high-k gate dielectrics in semiconductor devices, and later to complex ternary and quaternary perovskite oxides with novel functional properties. The most recent advancements related to the combined atomic/molecular layer deposition (ALD/MLD) have rapidly expanded the family of R-organic hybrid materials with intriguing luminescence and up-conversion properties. This review provides up-to-date insights to the current state of ALD and ALD/MLD research of R-based thin films and highlights their application potential.

1. Introduction

Atomic layer deposition (ALD) has been the fastest growing thin-film deposition technology in industry for decades. Since its development for industrial applications in the 1970s,^[1] it has become essential in various technologies in which high-quality, ultrathin and conformal inorganic coatings are needed.^[2,3] While in the past ALD was predominantly employed in the microelectronics sector, it is also strongly emerging toward many new application areas such as batteries,^[4] optoelectronics,^[5,6] solar cells,^[7-9] magnetics,^[10] and thermoelectrics.^[11] Material-wise, the ALD technique is fully versatile covering most of the elements in the Periodic Table;^[12,13] however, in the industrial applications of ALD, the variety of metal constituents has been so far mostly limited to a rather small fraction of the elements, mainly Al, Ti, Hf, and Zn.^[14-16]

Rare earth elements (Rs) comprise the 17 elements of scandium, yttrium, and the lanthanides (Ln; lanthanum and its 14 successors from cerium to lutetium) with gradually filled 4f orbitals. These elements are used in a variety of applications ranging from magnets, catalysis, and (optoelectronics to solar cells, lasers, and phosphors. The rare earth element chemistry is dominated by trivalent ions, particularly in the spectroscopy-related applications, such as light emitting diodes (LEDs), screens, night vision, and barcoding. These applications take the full advantage of the narrow-band high-intensity and color-pure emissions of the Ln³⁺ ions.^[17-21]

The ALD history related to the R-based thin films started in the early 1990s, when these elements were mainly applied as dopants in other thin films.^[22,23] Afterward, in particular during the first decade of the new millennium the interest in R-based ALD processes shifted to rare earth oxides investigated as potential high-k gate dielectrics in metal oxide semiconductor field-effect transistors (MOSFETs).^[6] In recent years, a renewed interest in R-based thin-film materials has been seen again. Increasingly complex material compositions have been studied, most prominently the perovskite-related oxides in which the rare earth elements are combined with d-block transition metals to facilitate interesting magnetic and catalytic properties. Also importantly, in this newly born research strive, a visible role has been played by the combined atomic/molecular layer deposition (ALD/MLD) technique,^[24-26] enabling hybrid lanthanide-organic thin films

A. Ghazy, M. Karppinen
 Department of Chemistry and Materials Science
 Aalto University
 FI-00076 Espoo, Finland
 E-mail: maarit.karppinen@aalto.fi

D. Zanders, A. Devi
 Inorganic Materials Chemistry
 Ruhr University Bochum
 Universitätsstr. 150, 44801 Bochum, Germany
 E-mail: anjana.devi@ruhr-uni-bochum.de

A. Devi
 Leibniz Institute for Solid State and Materials Research
 Helmholtzstr. 20, 01069 Dresden, Germany

A. Devi
 Chair of Materials Chemistry
 TU Dresden
 Bergstrasse 66, 01069 Dresden, Germany

A. Devi
 Fraunhofer Institute for Microelectronic Circuits and Systems
 Finkenstr. 61, 47057 Duisburg, Germany

 The ORCID identification number(s) for the author(s) of this article can be found under <https://doi.org/10.1002/admi.202400274>

© 2024 The Author(s). Advanced Materials Interfaces published by Wiley-VCH GmbH. This is an open access article under the terms of the Creative Commons Attribution License, which permits use, distribution and reproduction in any medium, provided the original work is properly cited.

DOI: [10.1002/admi.202400274](https://doi.org/10.1002/admi.202400274)

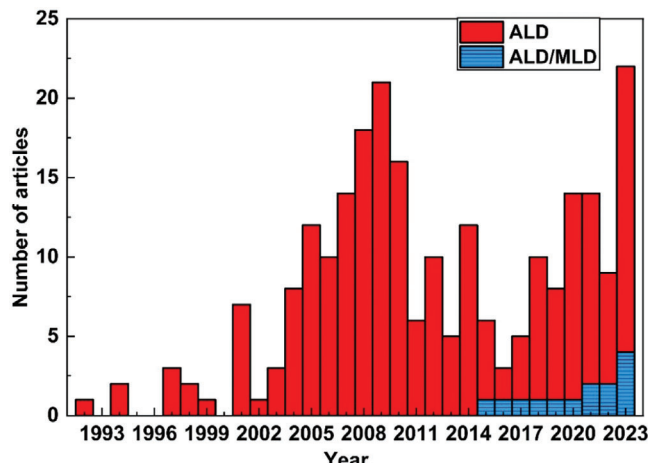


Figure 1. Annually published ALD and ALD/MLD articles involving rare earth elements from 1992 to 2023. The publications were searched from Scopus and Web of Science, using search terms that included “atomic layer deposition” and “rare earth”, or “atomic layer deposition” and “lanthanide”. The data thus acquired were further manually refined to check for numbers as accurate as possible. Data were accessed lastly on 10-02-2024.

with exciting photoluminescence (PL) and up-conversion (UC) properties.^[27] (Figure 1) plots the number of annually published ALD and ALD/MLD papers involving rare earth elements.

A significant challenge in the field of *R*-based ALD and ALD/MLD process developments has been the lack of distinctly superior precursors. For example, the first ALD processes for the R_2O_3 thin films were based on β -diketonate precursors, but suffered from the low growth rate, high carbon content, and the lack of large-area uniformity.^[28] The enthusiasm in developing novel *R*-based thin-film materials was temporarily stalled when the ALD-grown HfO_2 films overshadowed the R_2O_3 films in the gate dielectrics performance in microelectronics.^[29] The renewed research strive then has been fueled with efforts to build more complex material compositions in which the *R* species are used as dopants, as a complementary material layer in nanolaminate thin films, or in combination with organic precursors in novel metal–organic hybrid materials, which will be discussed later in this review.

Despite the continuous interest in the topic, there are no previous reviews on the use of ALD and MLD techniques for *R*-based thin films. In this review, we present a comprehensive account of the current state of research in the field, comprising not only the ALD-grown binary and ternary rare earth oxide processes but also the new metal–organic materials realized through ALD/MLD. We start with a brief description of the basics of the ALD and ALD/MLD techniques (Chapter 2), and a summary of the rare earth element precursors used (Chapter 3). Then in particular, efforts are made to summarize and discuss the use of *R*s as dopants in ALD (Chapter 4), followed by the ALD and ALD/MLD processes so far developed for *R*-based inorganic and metal–organic thin films (Chapters 5 and 6, respectively). These chapters are followed by a discussion of the potential applications of these *R*-containing thin films (Chapter 7). Finally, in Chapter 8 we give a brief outlook toward future perspectives and challenges in this field.

2. ALD and ALD/MLD in Brief

Atomic layer deposition is a state-of-the-art gas-phase fabrication technique for high-quality inorganic thin films. In ALD, the atomic-level control of the film growth is achieved by pulsing the gaseous/evaporated precursors into a vacuum reaction chamber alternatively, timely separated by an inert gas purging or a vacuum drawing step between two consecutive precursor pulses.^[1] This sequential precursor pulsing mode forms the basis for the unique ALD film-growth characteristics, i.e., self-terminated surface reactions and an atomic layer-by-layer growth mode, as well as large-area homogeneity and high-aspect-ratio conformity of the resultant thin films. The first industrial ALD applications emerged already in the late 1970s, based on some prototype binary metal oxide and sulfide processes.

In its simplest case, one ALD cycle consists of: i) metal precursor pulse, ii) N_2 purge to remove the excess precursor/reaction by-products, iii) second reactant pulse (e.g. H_2O or H_2S), and iv) N_2 purge to remove the excess precursor/reaction by-products, see (Figure 2).^[30] Ideally, one ALD cycle forms one monolayer of the targeted product; in practice, this monolayer growth is not always reached due to steric hindrance caused by large-sized ligands in the metalorganic precursor. Nevertheless, each ALD cycle should result in constant film growth.^[31] Hence, the growth of ALD films is usually expressed and evaluated in terms of a so-called growth-per-cycle (GPC) value. The cyclic precursor pulsing scheme is the originator of precise film thickness control.

The involvement of gas-phase chemicals only means that the resultant ALD thin films do not suffer from any solvent inclusion issues unfavorable in the case of traditional solvent-based thin-film fabrication techniques. Also, the fact that the precursors are allowed to saturate on the surface after each precursor pulse by controlling the pulsing and purging lengths properly is directly translated to the excellent film attributes (e.g. pinhole-free, smooth, uniform, and conformal).^[7] Finally, it should be emphasized that the modularity of individual ALD cycles allows the growth of more complex thin films as well, obtained by combining different binary ALD cycles in predetermined ratios. Indeed, various ternary and even quaternary processes have been developed, which have opened interesting prospects for multilayering and doping.^[32–34]

Originally, ALD was only used for inorganic materials, but in 1991 its organic counterpart, i.e. molecular layer deposition or MLD, was employed for the first time to obtain organic polymeric thin films with high thickness control.^[35] In recent years, the combination of these two techniques, i.e. the ALD/MLD technique, has been strongly emerging for the fabrication of different metal–organic and inorganic–organic multi-layer thin films.^[36–39] In ALD/MLD, gas-phase metal-bearing precursors and organic precursors are alternatively pulsed for the new hybrid structures. The metal components used in ALD/MLD already cover numerous elements from the different parts of the Periodic Table, i.e. s-block,^[12] p-block,^[40] d-block^[41,42] and f-block elements,^[43] while on the organic precursor side, a rapidly increasing variety of organic molecules have been tested based on aliphatic chains, aromatic rings, substituted rings and natural molecules such as nucleobases and curcumin.^[44–48] Even though the combined ALD/MLD is a relatively new approach, it has already offered a wide range of hybrid materials, both

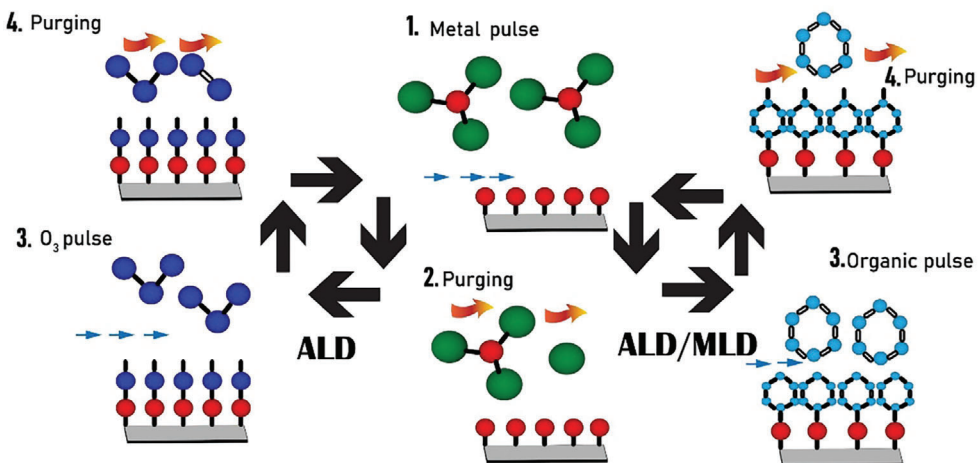


Figure 2. Schematic illustration of ALD and ALD/MLD precursor pulsing cycles, resulting in the growth of inorganic (left) and hybrid (right) thin films with atomic/molecular level accuracy: Red: metal; Green: precursor ligand; Blue: oxygen; Light blue: organics.

amorphous and crystalline,^[49] with application potential as e.g. battery materials, luminescent materials, thermoelectric materials, and porous metal–organic framework (MOF) materials.^[32]

In ALD processes, it is customary to look for a so-called ALD window within which the film-growth rate remains essentially independent of the deposition temperature. In ALD/MLD, such a temperature window is not usually found but the GPC value typically gradually decreases with increasing deposition temperature.^[2,50] Nevertheless, most of the ALD/MLD processes are fully controllable in a relatively wide temperature range. In general, compared to the ALD processes the GPC values are considerably higher for the ALD/MLD processes, owing to the larger-sized organic molecule constituents.

The ALD and ALD/MLD process developments for *R*-containing thin films comprise several crucial steps. The first step is the precursor choice (design and synthesis) which will be discussed in detail in the next chapter. A common practice in precursor development is to test the new precursors first in their corresponding R_2O_3 processes. Investigation of the self-saturation behavior is the most crucial step, as self-saturation is the main pillar of the ALD and MLD techniques, distinguishing them from the other chemical vapor deposition approaches.^[30] After confirming the self-saturation behavior of the precursor, the film-thickness control in relation to the number of ALD cycles applied at a given deposition temperature is tested in the second step. Such control is a direct result of the self-saturation behavior of the surface reactions.^[51] The third step of process development concerns investigations of the growth behavior at different temperatures, typically in the range of 100–300 °C.^[52] The temperature scanning is important for R_2O_3 thin films, as the deposition temperature impacts the properties of the films from crystallinity, impurities, and *R*:O ration.^[53,54] The development steps for the ALD/MLD processes are similar to those of ALD processes, as the two methods are analogous. However, an additional step is needed to confirm the surface saturation of the organic precursor. An example of process development results is shown in Figure 3.^[55]

3. Precursor Consideration

3.1. Rare Earth Element Precursor Chemistry

As indicated in the previous chapter, the chemical nature of a precursor and its physical properties can significantly impact the thin film growth during ALD or ALD/MLD processes, and thus also the properties of the resulting thin-film materials. Important aspects such as the reactivity toward a growth surface and a desired co-reactant, the film growth chemistry itself and created by-products, as well as thermal stability and volatility, needed for the vapor phase transport from a source vessel to the substrate surface, can be altered and adjusted by the choice and combination of the ligands comprising the precursor molecule.^[30,56,57]

The ALD history of *R*-based materials, first and foremost *R*-based binary and ternary oxides, spans more than three decades with pioneering works dating back to the mid to early 1990s.^[58–60] In this period of time, a broad variety of rare earth element precursors belonging to different compound classes have been successfully tested for ALD and ALD/MLD. (Figure 4) provides a schematic survey of these different *R* precursor classes that can be distinguished from one another based on the type of ligand(s) coordinating the central atom. Table S1 (Supporting Information) contains the references that this schematic and the entries in subsequent (Figure 5) are based on. Appreciably, representatives of these classes have found more and more use for the ALD of a broader material range beyond oxides, namely nitrides, sulfides, fluorides, or inorganic–organic hybrids in recent years.^[61–64]

A focal point dominating the initial phase of rare earth ALD expansion alongside precursor and process development was however the need to find a gate dielectric replacement for silicon dioxide (SiO_2) with a notably higher dielectric constant in MOSFETs by the mid-to-late 2000s.^[65,66] At that time, some of the *R*-based oxides grown by ALD ranged among the most promising contenders for an alternative high-k material in the semiconductor industry even though hafnium dioxide (HfO_2) was eventually favored for gate insulator applications.^[67,68] Albeit, these “high-k

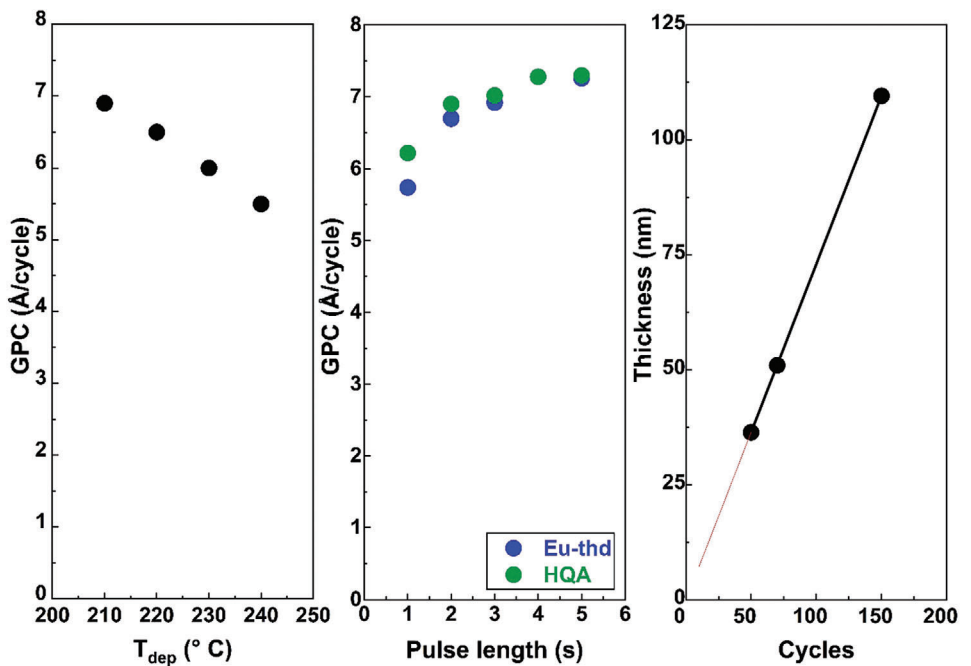


Figure 3. Process development steps of Eu-HQA thin films that show temperature scanning (left), surface saturation of precursors (middle), and thickness control over the number of ALD/MLD cycles (right). (Reproduced under CC licence from ref. [55], 2023, Royal society of chemistry).

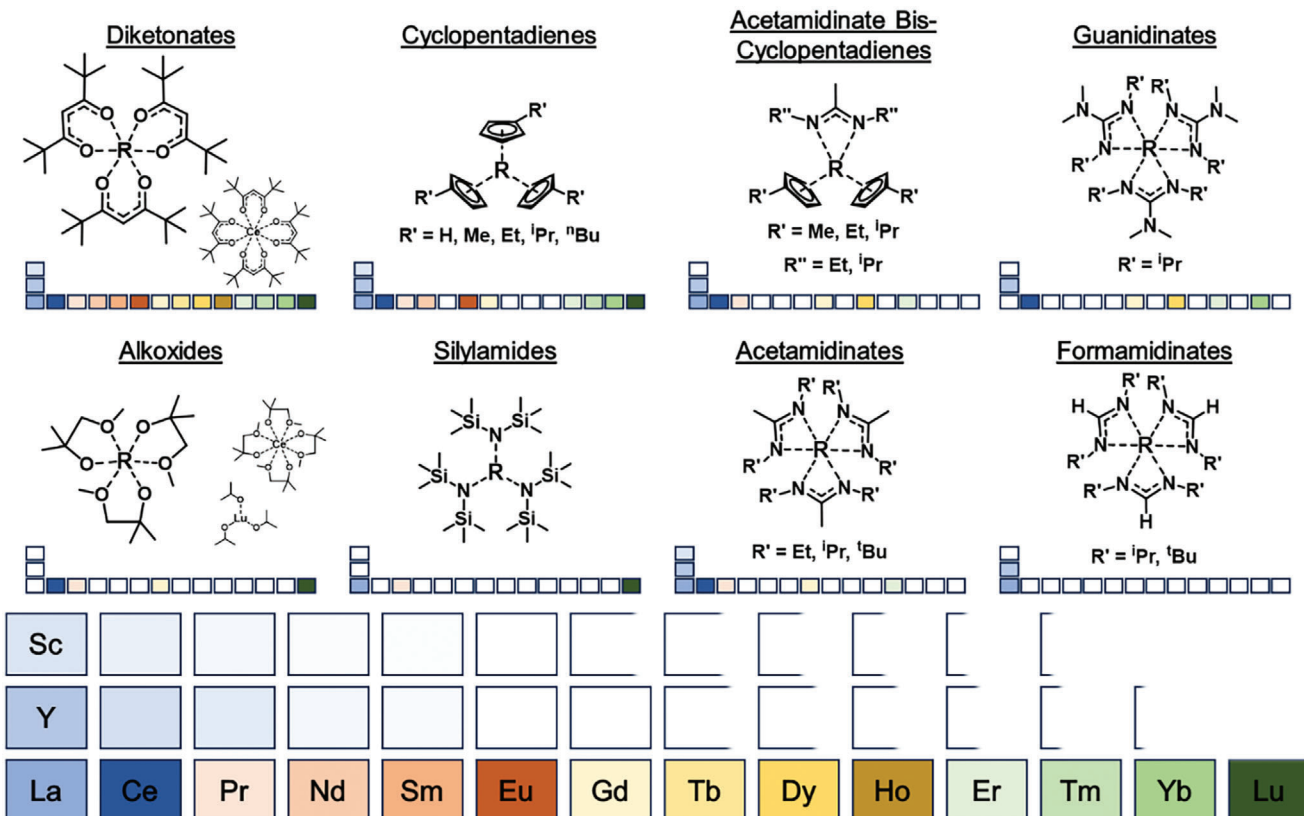


Figure 4. Survey over the different rare earth precursor classes commonly employed for the ALD and ALD/MLD of rare earth containing thin films. Color bars indicate successful ALD employment of the compound class for the respective element. R represents an element of the extended rare earth elements, while R' and R'' refer to specific substituents. These are: H = Hydrogen, Me = Methyl, Et = Ethyl, iPr = Isopropyl, nBu = Butyl, tBu = Tert-butyl.

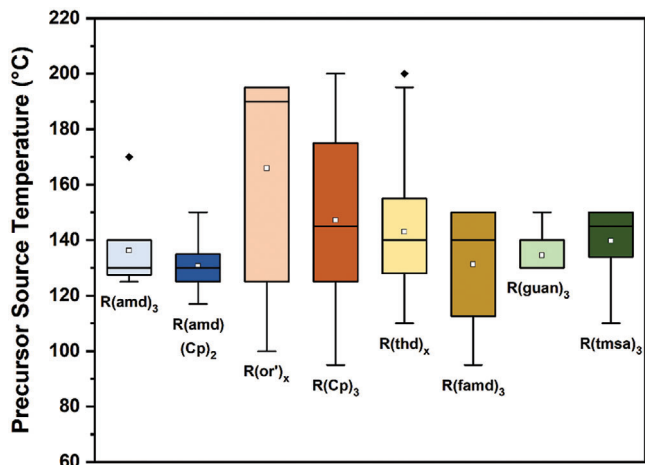


Figure 5. Box plots for the precursor vessel temperatures for the prior introduced precursor classes. Boxes contain the average 50% of the respective dataset while white dots represent the arithmetic mean. The first quartile is the median of the lower half of the dataset, and the third quartile is the median of the upper half of the dataset. The whiskers are restricted to a 1.5x inter quartile range representing entries outside the box. Outliers are depicted as black dots. If lower or upper whiskers are not displayed an overlap with the respective quartile occurred.

considerations" affected the assessment of novel *R*-based ALD precursors and processes for a period of time.

The by far most extensively employed precursor class is one of the β -diketonates of which complexes for all the 17 rare earth elements have been synthesized and employed in ALD. Hereby, the β -diketonate ligand, more specifically 2,2,6,6-tetramethyl-3,5-heptanedionate (thd), is characterized by its chelating nature, steric demand that effectively shields the central atom and strong bonding between its oxygen atoms and *R* elements.^[69,70] Notably, many *R* compounds ligated by the lighter β -diketonate pentane-2-4-dione or simply acetylacetone are only stabilized in hydrated form and display strong intermolecular interactions.^[71,72] These interactions aggravate volatilization and loss of hydrate ligands as well as thermal instability of the remaining *R* compound impede controlled vapor transport which has rendered the use of *R*(pentane-2-4-diones)_x in ALD unfavorable.^[73,74] On the other hand, fluorinated β -diketonate ligands such as 1,1,1,5,5-hexafluoropentane-2,4-dionate (hfac) were neither suitable for *R* precursors in ALD as prior low-temperature CVD (chemical vapor deposition) studies had already highlighted the problem of unwanted fluorine incorporation in *R*-oxide thin films.^[75]

Likewise, often employed and tested for the majority of the *R* elements is the cyclopentadienyl class. The so-called Cp ligands distinguish themselves through η^5 -bonding from their ring carbon atoms to the *R* atom.^[76,77] Typically employed Cp ligands for the coordination of *R* precursors may display a number of alkyl ring substituents ranging from methyl over ethyl to isopropyl to alter intermolecular interactions and thus adjust relevant properties such as melting point, volatility, and even reactivity. Exemplarily, Blanquart et al. showed for a group of Er tris cyclopentadienyl precursors with varying Cp substituents (Me, ⁱPr, ⁿBu) in a detailed ALD process study with H_2O and O_3 as the co-reactants that the processes employing the ⁿBuCp ligated Er pre-

cursor outperformed the others in terms of the GPC and film conformality.^[78]

Two other precursor classes that experienced astir interest, especially in the earlier days of *R*-based ALD are the alkoxides and silylamides. Rare earth precursors for a selected number of *R* elements were synthesized and tested in proof-of-concept ALD studies.^[79–81] The reasoning behind studying precursor classes other than the $R(thd)_x$ and $R(Cp)_3$ originated firstly from the effort to employ less harsh co-reactants and lower temperatures for the deposition of high-quality oxide thin films and second from the perception of the low volatility of the established precursor classes.

Factually, $R(thd)_x$ precursors were shown to not properly work with H_2O as co-reactant and to require rather high deposition temperatures of 300 °C or more with ozone as counterpart to yield thin films displaying appreciable crystallinity and composition.^[82,83] With these O_3 -based processes only moderate GPCs in the range of 0.1–0.4 Å were achieved and minor carbon impurities remained in the grown thin films.^[28,84] Most profoundly however, the use of O_3 caused typically the formation of a pronounced interfacial layer between the *R*-oxide film and Si/SiO_2 substrates with ill-defined stoichiometry and overall poor dielectric properties (low permittivity, leakage).^[85] This rendered a notable problem for integration for the gate insulator application. Contrastingly, various $R(Cp)_3$ precursors were implemented successfully in ALD processes in combination with H_2O , however at the expense of other shortcomings: at low deposition temperatures ranging from 150 to 250 °C the GPC in $RCp_3 + H_2O$ processes were found to be already in an appreciable range of 0.8–1.2 Å. But typically, the thin films displayed crystalline domains while being oxygen-rich and containing notable amounts of carbon and especially hydrogen.^[86,87] This rendered problematic in as much as that the disreputable role of non-ideal stoichiometry and hydrogen in the creation of defects in high-k dielectrics and devices based on them was a known issue.^[88,89] For films grown with H_2O above 250 °C, carbon and hydrogen contents decreased while GPCs often increased to and above 1.5 Å (even 2.0 Å) which raised suspicion regarding premature precursor decomposition and the true self-limiting nature of some of the ALD processes.^[78] Clearly, H_2O prevailed as the preferred co-reactant for *R*-based oxides and $R(Cp)_3$ precursors had shown some promise, but ultimately did not provide the right reactivity to facilitate the growth of crystalline, stoichiometric, and hydrogen-deficient thin films. This ultimately led to the investigation of rare earth alkoxides $R(or')_x$ and silylamides $R(tmsa)_3$ as precursor classes with lower acidity of the protio-ligand allowing for higher reactivity toward H_2O .^[90]

After initial precursor and process development for a limited number of rare earth elements, the choice had to be re-evaluated, however. In the case of the $R(tmsa)_3$ precursor family specifically relying on the bis(trimethylsilyl)amido (tmsa) ligand, it may have been reasoned that silicon being part of the ligand sphere and near the central metal would have a positive stabilizing effect as known from synthetic, liquid phase chemistry for complexes across the Periodic Table.^[91,92] Experimentally, the opposite was demonstrated by Scarel et al. in the example of an ALD study using $Lu(tmsa)_3$ and H_2O .^[81] By analysis of the molecular solid-state structure of the precursor an agnostic interaction, a three-centre two-electron interaction,^[93] spanning from the

trimethylsilyl Si across the amido N to the central Lu atom. Based on this observation it was hypothesized that metal centers in $R(tmsa)_3$ precursors were coordinatively undersaturated paving the path for weakening their R–N bonds by this interaction. Practically this was reflected by the significant incorporation of Si but also C with little control over the exact quantity in all ALD studies for the deposition of R-based oxides employing $R(tmsa)_3$ compounds irrespective of the co-reactant choice.^[81,94,95] Based on experimental insights, the compound class was furthermore suspected to only possess limited thermal stability and tend toward premature decomposition as truly self-limiting film growth was not observed, especially for temperatures exceeding 200 °C.^[52,94]

Closer performance evaluation of $R(or')_x$ precursors in ALD for a selected number of Rs ranging from Ce and Pr over Gd to Lu showed mixed results. Notably, most studies relied not on conventional but liquid injection ALD. Despite the appreciable short-term volatilization behavior of the compounds assessed by thermogravimetric analysis (TGA), their overall stability and shelf-life when heated were found to be poor and impeding vapor phase transport. Thus, a stabilizing solvent had to be applied.^[85,96] Too high a reactivity also rendered problematic for the film growth of R-based oxides. While for some of the $R(or')$ precursors the onset of CVD contributions was observed at temperatures around 300 °C,^[85] for other temperatures were as low as 225 °C.^[96] Commonly, the tendency of the compounds to undergo β -hydrogen elimination was seen as the root cause preventing self-limiting film growth. Regardless of the CVD contributions to film growth, a broad temperature window ranging from 200 to 400 °C was screened for their use together with H_2O in several studies. $R(or')$ precursors typically demonstrated decent reactivity with H_2O even at low process temperatures falling below 200 °C, but the resulting layers contained high levels of hydrogen impurities deteriorating their dielectric properties.^[97] For films grown above 300 °C, hydrogen contents diminished but the layers were either oxygen-deficient or oxygen-rich leading to poor control over film stoichiometry.^[96,97]

Seeking to find a better balance between the stability and reactivity of R precursors with improved volatilization behavior compared to $R(thd)_x$ and $R(Cp)_3$ complexes, all-nitrogen coordinating, chelating ligands such as acetamidates (amds), guanidates (guans) and formamidates (famds) were subsequently employed in the synthesis of alternative precursor candidates. The introduction of the acetamidate ligand to rare earth precursor chemistry dates back to 2003 when Lim, Gordon, and co-workers demonstrated the first ALD processes exploiting this new precursor class.^[98,99] For R compounds, a threefold coordination by the N,N'-chelating ligand with varying alkyl substituents at the coordinating nitrogen atoms was observed and subsequently, oxide ALD processes were developed for a couple of Rs ranging from Y, Sc, and La to Ce, Pr, Gd, and Er.^[100–105] ALD studies were typically conducted between 150 and 300 °C with either H_2O or O_3 as co-reactant. While H_2O dosing facilitated self-limiting film growth in combination with Et and tPr sidechain substituted $R(amd)_3$ precursors, tBu substituted precursor congeners required O_3 as co-reactant to enable film growth. Water-based processes typically facilitated appreciable GPCs of $\approx 1.0 \text{ \AA}$ and due to the high reactivity toward H_2O , film growth was observed at temperatures as low as 150 °C in some cases. Overall, carbon and nitrogen contaminant levels were found to be low

but many of the thin films were oxygen-rich. This was associated with incomplete reactions with the co-reactant and the formation of hydroxyl groups in the film bulk. As a rule of thumb, it was found that the lower the deposition temperature was, the higher the over-stoichiometry of oxygen. It turned out to be a conflicting correlation as the onset of decomposition for $R(amd)_3$ precursors was found to be between 275 and 300 °C in H_2O -based ALD processes. Thus, congeners of the $R(amd)_3$ precursor class experienced increased interest.

While the amd ligand exhibits an alkyl group, typically Me, at the central backbone carbon, the guan ligand displays a dialkylamino function there and in the case of the famd ligand it is only a H atom. These differences, while being subtle, were shown to have a profound impact on electron delocalization within the ligand and thus its bonding behavior as well as on the steric demand of precursor fragments adsorbed to the surface alongside the reaction rate with H_2O .^[57,106] $R(guan)_3$ compounds were synthesized and tested for similar Rs than in the case of the $R(amd)_3$ precursor class with the addition of Dy and Yb.^[54,105,107–109] Furthermore, they were successfully employed in ALD/MLD hybrid material growth studies.^[61,110] Just as for R oxide ALD processes using $R(amd)_3$, film growth studies with $R(guan)_3$ precursors in interplay with H_2O were conducted between 150 and 300 °C. Self-limiting growth characteristics with GPCs $\approx 1.0\text{--}1.3 \text{ \AA}$ were typically found between 200 and 250 °C. At and above 275 °C however partial precursor decomposition was observed that manifested itself first in a step increase of the GPCs and then $\approx 300 \text{ °C}$ in an even steeper decline. For R_2O_3 thin films grown under optimized conditions, carbon and nitrogen contamination levels were generally low in the film bulk and the films displayed almost ideal stoichiometry with minor oxygen excess. Yet, the layers were only moderately crystalline, and the extent of hydrogen contamination was not investigated systematically. Proof of concept dielectric property characterization in metal oxide semiconductor (MOS) capacitor structures, yielded mixed results. For some of the R oxide films (5–10 nm thickness), dielectric constants were notably lower than for bulk materials, and interface trap densities were likewise considerable. Yet, good performance was demonstrated in selected cases. Overall, capacitor post-treatment exemplarily by forming gas annealing allowed to realize performance improvements, while higher initial deposition temperatures would have been the preferred choice to circumvent post-treatments. Mechanistic studies however unraveled the cause for the decomposition of $R(guan)_3$ precursors in ALD above 275 °C to be carbodiimide de-insertion which illustrated one limitation of this precursor class.^[111,112]

Up to this point, only a few selected $R(famd)_3$ precursors, namely for Y and La, and their employment in ALD have been presented.^[53,113,114] Nonetheless consideration of this compound class is justified as prior comparative studies on amd and famd ligated precursors and their process performance hinted toward potential advantages of the latter over the former. It was hypothesized that the smaller and less hydrophobic famd ligand and precursor molecules based on it would allow for faster and more complete reactions with H_2O in oxide processes.^[106] Boysen et al. expanded this comparison to $Y(guan)_3$ and $Y(famd)_3$ precursors in systematic studies.^[53,114] Overall, more crystalline Y_2O_3 thin films with considerably higher density could be grown. The famd ligation allowed to advance to process temperatures of 325 °C

while self-saturating growth behavior was maintained. Consequently, the films demonstrated close to ideal Y:O ratio and a lower hydroxyl content in the film bulk. In direct comparison to Y_2O_3 thin films prior grown from $\text{Y}(\text{amd})_3$ precursors, various process and material property improvements became apparent. The most notable one was an increase of the dielectric constant for films in MOS capacitor structures to 13.9 accompanied by low interface trap densities and appreciably high breakdown fields.

While $\text{R}(\text{amd})_3$, $\text{R}(\text{guan})_3$, and $\text{R}(\text{famd})_3$ precursors aroused notable academic interest over the years and found frequent employment in proof of concept studies, there is one other precursor class that did not only do that but also succeeded in becoming large-scale manufacturable and thus industrially relevant: this precursor class comprises heteroleptic $\text{R}(\text{amd})(\text{Cp})_2$ compounds that were designed to find a good trade-off between thermal stability and adjusted reactivity. Currently, $\text{R}(\text{amd})(\text{Cp})_2$ precursors with varying alkyl side chains at both ligands have been devised and evaluated for a couple of Rs such as Y , La , Ce , Pr , Gd , Dy , and Er .^[78,115–120] As intended, the $\text{R}(\text{amd})(\text{Cp})_2$ precursor class was found to outperform $\text{R}(\text{Cp})_3$ precursors in H_2O -based ALD processes by a large margin in terms of film purity and required growth temperatures. For self-limiting film growth, temperatures typically ranging between 200 and 250 °C were reported, but in some cases, ALD type growth was even shown at higher temperatures such as 300 °C. The GPCs ranged from 1.0 Å even up to 2.0 Å. As Seppälä et al. previously observed, there appeared to be a correlation between the ionic radius of the central metal and the thermal stability of the respective $\text{R}(\text{amd})(\text{Cp})_2$ complex whereby later decreased with increasing ionic radius.^[118] Despite the apparent variation in thermal stability and accessible ALD temperature range, $\text{R}(\text{amd})(\text{Cp})_2$ precursors were still found to be on par or even better than respective $\text{R}(\text{amd})_3$ or $\text{Ru}(\text{guan})_3$ congeners in terms of grown R_2O_3 oxide thin film quality. A key differentiator between the $\text{R}(\text{amd})(\text{Cp})_2$ class and all other precursor classes previously mentioned was identified in the exceedingly low melting points of the heteroleptic compounds. Already at room temperature most of the to-date reported $\text{R}(\text{amd})(\text{Cp})_2$ complexes are liquid while other R precursors remain solid even when being heated under operational conditions except for some $\text{R}(\text{Cp})_3$ compounds.^[121,122]

As detailed above, R precursor classes have been developed with different types of ligands and display a variety of different bonding motives and differences in the periphery of the respective ligands which allows to alter properties such as aggregate state, chemical reactivity, and volatility. The latter is of crucial importance but is typically only estimated and evaluated from TGA which the mass loss due to evaporation or premature decomposition is monitored as a function of a programmed temperature increase.^[123] While TGA is a powerful tool for the initial and comparative assessment of the suitability of precursor candidates for gas phase deposition techniques,^[124] insights originate from isolated and individual measurements with small quantities of analyte under conditions very different from the actual use case in ALD reactor systems. Consequently, information obtained from TGA can only serve as a starting point for precursor delivery settings such as the vessel temperature in ALD systems, and e.g. a 1 Torr vapor pressure temperature derived for a precursor by TGA might often not represent the actual heating temperature for the compound under use conditions. Besides, no consistent

database on either TGA information or heating settings exists for R precursors that allow for a fast survey.

To begin to address this situation, we display in (Figure 5) a survey of the source temperatures employed for a multitude of R precursor belonging to the prior discussed classes. The depicted Box plot representation is meant to provide a simple, comparative impression of the used vessel temperatures for each precursor class, averaged over all respective R elements, across reactor systems and under operational conditions. Table S1 (Supporting Information) contains all the entries and references that were consulted for this analysis. Furthermore, the SI contains a variant of Figure 5 illustrating the distribution of entries for every precursor class (Figure S1, Supporting Information). Box plots identical to Figure 5 for the most often used $\text{R}(\text{thd})_x$ and $\text{R}(\text{Cp})_3$ precursor classes that differentiate between the individual rare earth elements are also provided (Figures S2 and S3, Supporting Information).

Exemplarily, such a statistical approach allows us to consider established perceptions like the earlier mentioned one on the comparably low volatility of the $\text{R}(\text{thd})_x$ and $\text{R}(\text{Cp})_3$ precursor classes compared to others and the respective implications toward precursor delivery parameters such a source heating from a different perspective. Indeed, the herein presented analysis shows that this discernment is only partially justified. The arithmetic means for most of the precursor classes are interestingly located in a narrow 16 °C window encompassing the entries for $\text{R}(\text{amd})(\text{Cp})_2$ (131 °C), $\text{R}(\text{famd})_3$ (131 °C), $\text{R}(\text{guan})_3$ (134 °C), $\text{R}(\text{amd})_3$ (136 °C), $\text{R}(\text{tmsa})_3$ (140 °C), $\text{R}(\text{thd})_x$ (143 °C) and $\text{R}(\text{Cp})_3$ (147 °C). Only $\text{R}(\text{or})_x$ precursors display notably higher arithmetic means for the source temperature of 165 °C. A closer consideration via box plot analysis of source temperatures for the $\text{R}(\text{thd})_x$ (Figure S2, Supporting Information) and $\text{R}(\text{Cp})_3$ (Figure S3, Supporting Information) precursor classes with differentiation between individual rare earth elements revealed between the two: for $\text{R}(\text{Cp})_3$ precursors variation in the applied source temperatures in dependency of the elements but no clear trend was found. Contrastingly, for $\text{R}(\text{thd})_x$ precursors a decrease of the arithmetic applied temperature with decreasing ionic radii was observed.

This example does by no effect question the differences in the volatility of precursors having their arithmetic means within the 16 °C temperature window but may be seen as an encouragement to not outweigh volatility data differences as they may not affect the use condition parameter source temperature proportionally. Certainly, other and more nuanced considerations can be made based on the introduced box plot analysis but lie beyond the scope of this review which aims to introduce another tool to link fundamental experimental data with practical thinking.

To conclude, a summary table is provided to allow for a very concise, yet simplified comparison between the different rare earth precursor classes introduced and discussed in this chapter. The discussion provided throughout this chapter is the basis of Table 1, which lists several categories in which the precursor classes are rated from “–” corresponding to comparatively poor performance to “++” indicating average performance and “++” expressing better than average performance. The criteria are “commonness” expressing how many of the members of the extended rare earth element family compounds of the respective classes have successfully been employed in ALD.

Table 1. Comparative rating of the different rare earth precursor classes in various aspects ranging from availability over physico-chemical properties to ALD technique-related aspects.

Precursor Class	Commonness	(Thermal) Stability	Reactivity	ALD Performance	ALD/MLD Prospect
$R(\text{amd})_3$	+	+	+	+	+
$R(\text{amd})(\text{Cp})_2$	+	++	+	++	+
$R(\text{Cp})_3$	++	++	+	+	○
$R(\text{famd})_3$	-	+	++	++	++
$R(\text{guan})_3$	○	+	+	○	+
$R(\text{or}')_x$	-	-	-	-	-
$R(\text{thd})_x$	++	++	○	+	++
$R(\text{tmsa})_3$	-	-	-	-	-

Secondly, the “(thermal) stability” and shelf-life information available are ranked alongside the overall “reactivity” of the precursor classes with respect to co-reagents such as H_2O . The demonstrated “ALD performance” in the reported processes is naturally another crucial aspect. Here, the focus is placed on how well the precursor classes enabled truly self-limited film growth. The last category, namely “ALD/MLD prospect” aims to give an outlook on how suitable precursors from the different classes might be for the hybrid film growth. This category is the most difficult one to make clear statements for as to this date significantly less ALD/MLD than ALD processes have been reported and fewer precursors have been tested for the former. However, knowledge of the reactivity of the different precursor classes and their reported ALD performance thus far allows for educated predictions in cases where ALD/MLD processes have not yet been reported.

3.2. Co-Reactants in the Rare Earth Element-Based Processes

Most of the R -based ALD processes reported are oxide processes, and an evident issue related to the oxide films has been that the $R(\text{thd})_3$ precursors so far most commonly used for the ALD growth of R_2O_3 films (as they are easy to handle) lack the reactivity with H_2O .^[58,125] Instead, the $R(\text{thd})_3$ precursors require a strong oxidizing agent such as ozone, as the co-reactant. Even with ozone, the GPC values are relatively low, ranging from 0.45 Å for Nd_2O_3 down to 0.13 Å for Sc_2O_3 .^[125,126] At low deposition temperatures the processes yield amorphous or poorly crystalline films, and the carbon content of the films is usually high. Hence to obtain higher-quality films, the depositions are usually performed at $\approx 300^\circ\text{C}$.^[28,124]

Cyclopentadienyl-based precursors show higher reactivity toward water thus removing the need to use strong oxidizing agents for the growth of R_2O_3 films. In fact, using ozone with cyclopentadienyl precursors often leads to higher carbon contamination as the Cp ring decomposes in the presence of strong oxidizing agents; with mild oxidizing agents such as water, only the metal–carbon bond is broken, as desired. With cyclopentadienyl-based precursors, the GPC values are typically appreciably high, e.g. 1.7 Å in the case of Y_2O_3 films deposited from ethyl-substituted $\text{Y}(\text{Cp})_3$ and water, though within a relatively narrow temperature range of 250–285 °C only.^[127] When $\text{Y}(\text{PrCp})_3$ was combined with ozone, the same growth rate was obtained but within a wider

temperature window of 240–300 °C. However, the films had higher carbon content, and a post-deposition treatment was required to remove it.^[128] Water has been used as a co-reactant also with homoleptic amidinate, formamidinate, and guanidinate-based rare earth precursors, to obtain the following growth rates for the resultant R_2O_3 films: 1.05 Å with $\text{La}(\text{Pr}_2\text{amd})_3$,^[129] and 0.8 Å with $\text{Y}(\text{Pr}_2\text{amd})_3$. While the carbon content remained low, the films were found to contain a slight oxygen excess.^[100] For the $\text{Y}(\text{Pr}_2\text{famd})_3 + \text{H}_2\text{O}$ process, the GPC value was high (1.36 Å) but no stable deposition temperature window was found, and the films showed higher than expected oxygen content ($\text{O}:\text{Y} = 1.7$) when deposited at 300 °C; this ratio increased up to 2.0 when the films were deposited at 250 °C or lower. On the other hand, increasing the deposition temperature to 325 °C decreased the $\text{O}:\text{Y}$ ratio to 1.6, which is closer to the ideal stoichiometry of 1.5.^[53] In (Figure 6) we show two comparisons, in one we highlight the different growth rates of Y_2O_3 thin films deposited by ALD from various Y^{3+} precursors upon using water as a co-reactant, and another comparison shows the effect of varying the co-reactant with the same Y precursor on the growth rate of Y_2O_3 thin films by ALD.

A promising water-assisted process has been reported for Y_2O_3 films based on the $\text{Y}(\text{Pr}_2\text{amd})(\text{PrCp})_2$ precursor;^[119] in first research the GPC value was ≈ 0.5 Å at 350 °C, but later significantly higher growth rates (1.3 Å) were reported at the same deposition temperature.^[118] The La-counterpart, i.e. $\text{La}(\text{Pr}_2\text{amd})(\text{PrCp})_2$ was tested with several different oxidants, and the results revealed CVD-type formation of $\text{La}(\text{OH})_3$ with a higher than expected growth rate up to 3.0 Å at 300 °C, in particular when the purging length of water was decreased from 20 to 10 s. Similarly, no constant GPC temperature window was found with ozone, ethanol, or ozone + water mixture as the co-reactant. However, with the ozone + water mixture, the surface saturation was evident.^[116]

In the few non-oxide R -based ALD processes reported so far, $R(\text{thd})_3$ has been a typical choice for a metal precursor. From $R(\text{thd})_3$ precursors in combination with H_2S as the sulfur source, La_2S_3 , and $\text{Y}_2\text{O}_2\text{S}$ films have been grown.^[130,131] Recently, several fluoride (RF_3) processes have been developed using various fluorine sources, such as TiF_4 and NbF_5 . The use of these transition metal fluorides as the F source has however in some cases left traces of these metals in the films, while in some other cases when using relatively high deposition temperatures ($\approx 300^\circ\text{C}$) no metal contamination traces were detected.^[132–134]

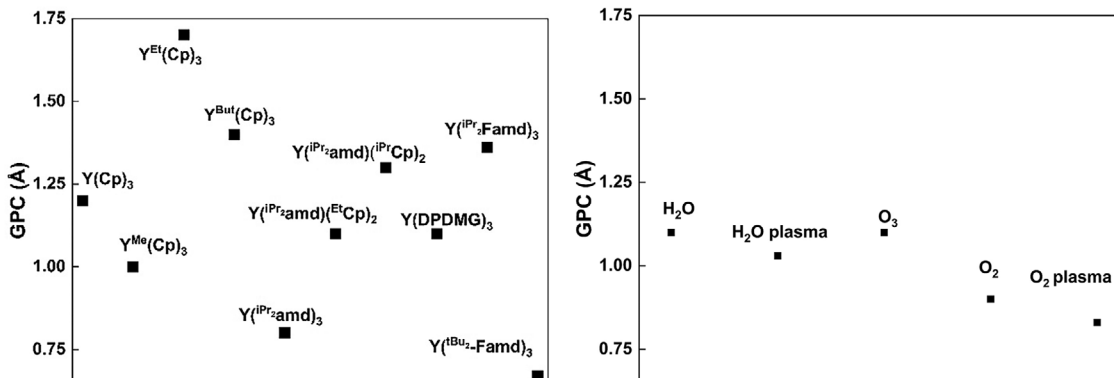


Figure 6. Growth rates of different Y_2O_3 processes (left) with different Y-precursors and H_2O as co-reactant, and (right) with different co-reactants and $\text{Y}(\text{iPr}_2\text{amnd})(\text{EtCp})_2$ as Y-precursor.

4. Rare Earth Elements as Dopants in ALD

Trivalent Ln^{3+} ions are renowned for their luminescence properties. Their 4f electrons are efficiently shielded from the coordination environment by the spatially more extended 5s and 5p orbitals, which allows the emission to be independent of the host lattice, resulting in narrow and color-pure emission bands. Additionally, the parity-forbidden nature of their f-f transitions leads to long luminescence lifetimes ranging from μs to ms. In UV-excited photoluminescence applications, the most commonly used lanthanide ions are Tb^{3+} for green emission and Eu^{3+} for red emission. On the other hand, some of the lanthanide ions such as Ho^{3+} and Er^{3+} are known for their up-conversion properties: UC Ln^{3+} ions are able to absorb two or more photons sequentially, and then emit a single higher-energy photon with a lower wavelength.^[18] This can be employed for converting NIR radiation into visible light, and potentially utilized in applications such as photovoltaics and biological imaging.^[27] A feature common to both PL and UC materials is that the Ln^{3+} ions suffer from a so-called concentration quenching phenomenon which suppresses the emission rapidly with increasing concentration of the luminescent species. Hence, the Ln^{3+} ions are often diluted for different PL and UC applications by embedding them as dopants in a suitable host lattice.

Doping in ALD thin films is generally realized through a so-called supercycle concept (Figure 7).^[135] In an ALD supercycle, the order and number of cycles of two or more metal precursors can be freely chosen, according to the targeted composition in the thin film material aimed for. Ideally, this provides a route to a well-controlled composition doping, but in practice, there are several challenges related to such multicomponent films to be taken into account, most significantly the different reactivities and sizes (steric hindrance) of the ligands in the different metal precursors.^[136] It is quite common to apply a full ALD cycle (dopant-metal precursor + co-reactant) for the dopant metal, i.e. (main-metal \rightarrow co-reactant \rightarrow dopant-metal \rightarrow co-reactant), but it is possible to pulse the dopant-metal precursor directly after the main-component metal precursor, i.e. (main-metal \rightarrow dopant-metal \rightarrow co-reactant). However, in the latter case, unwanted dopant-to-metal exchange reactions are often seen.^[137]

Another fundamentally different doping strategy is to use a single multi-metal precursor. This multi-metal precursor could

be originally synthesized (e.g. through co-precipitation) from the two metal constituents or just simply mechanically mixed from the two independent metal precursor powders in the desired ratio.^[138]

In the latter case, also sometimes named “co-dosing” it is somewhat challenging to achieve perfect composition control, particularly when the different precursor powders possess significantly different vapor pressures, which often leads to a final film composition that is different from the initial mixing composition.^[139,140]

Lanthanide-doped ALD films were first reported in 1992 for Tb^{3+} -doped (2%) ZnS films,^[22] and a little later for CaS films

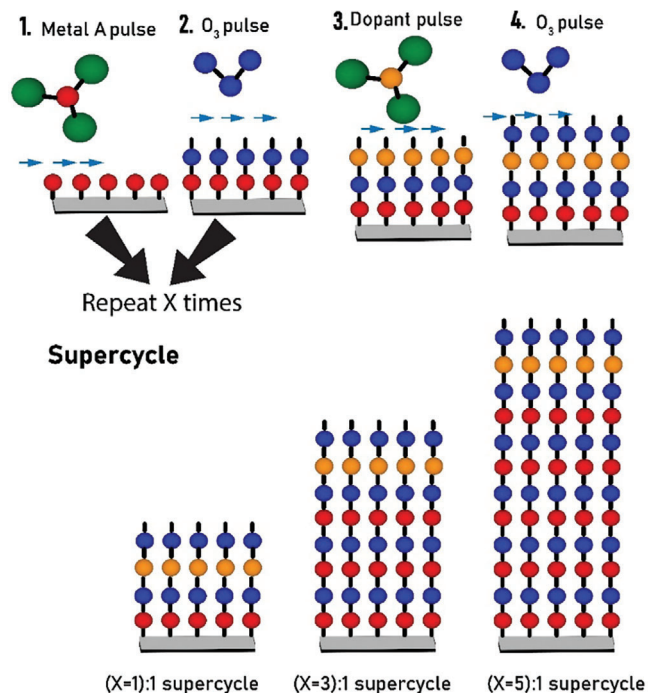


Figure 7. Supercycle concept for doping in ALD: in the simplest case the supercycle consists of x cycles of the main metal and one cycle for the dopant metal, but the supercycle may also include several cycles of the dopant metal or several different metal-dopant.

Table 2. Use of different R species as dopants in ALD.

Material	Dopant	Application	Refs.
ZnS	Tb	Luminescence	[22]
CaS	Tb, Ce, Eu	Luminescence	[23,64]
SrS	Tb, Ce	Luminescence	[154]
Al ₂ O ₃	Er, Yb, (Er,Yb)	Waveguides, Luminescence	[144,147,155,156]
Y ₂ O ₃	Er, Eu	Luminescence	[146,157–160]
Y ₃ Ga ₅ O ₁₂	Er	Luminescence	[161]
ZrO ₂	Y, La, Dy	Electrolyte, Interphase	[137,151–153,162,163]
HfO ₂	Y, La,Pr, Gd, Er,Dy	Gate dielectrics, Memory	[164–176]
HfO ₂ /ZrO ₂	Y, La, Gd.	Memory	[177]
Ga ₂ O ₃	Nd,Er	Luminescence	[145,178]
GeO ₂	Er	Luminescence	[179]
Yb ₂ O ₃	Er	Luminescence	[148]
TiO ₂	La, Pr, Nd, Sm, Eu, Tb, Dy, Ho, Er, Tm, Yb	Magnetics, Luminescence	[180,181]
Yb _x Ti _y O _z	La, Pr, Nd, Sm, Eu, Tb, Dy, Ho, Er, Tm	Luminescence	[181]
YDC	Y	Electrolyte	[136,182]
SrTiO ₃	La	Gate dielectrics	[183]
Y ₂ O _{3-x} S _x	Eu	Luminescence	[184]
YVO ₄	Nd, Sm, Eu, Tb, Dy, Ho, Er, Tm, Yb	Thermometry	[141,142]
Gd ₃ Ga ₅ O ₁₂	Er	Luminescence	[185]
Yb ₃ Al ₅ O ₁₂	Er	Luminescence	[149]
Lu ₃ Al ₅ O ₁₂	Er	Luminescence	[150]
ZnGa ₂ O ₄	Er	Luminescence	[186]
SrSnO ₃	La	Optoelectronics	[187]

doped with different concentrations of Ce³⁺, Tb³⁺, and Eu³⁺.^[23] More recently, the emission wavelength of Eu³⁺ in CaS was shown to be tunable by means of introducing oxide ion defects, thereby increasing the oxidation state of Eu.^[64] This was achieved by replacing the Eu(thd)₃ + H₂S cycle for CaS:Eu films with the Eu(thd)₃ + O₃ cycle for CaS:Eu-O films. It was found that the emission wavelength of the CaS:Eu films (647 nm) was blue-shifted by ca. 20 nm compared to the CaS:Eu-O films (625.8 nm). Such a defect control as achieved here might be difficult to achieve by other synthesis techniques. Table 2 below shows a list of the use of R metals as dopants in ALD thin films.

Recently, luminescent Ln³⁺-doped YVO₄ films were reported with promising optical thermometry performance. In these depositions, the Ln³⁺-doping level was carefully optimized through the supercycle approach by controlling the cycle sequence of Y(thd)₃, VO(thd)₂, and Ln(thd)₃ precursors.^[141,142] Similarly, UC thin films with proper Ln³⁺-doping have been investigated. For example, slightly Er³⁺-doped (3%) Yb₂O₃ films showed exciting two- and three-photon UC phenomena when excited by a $\lambda = 974$ nm laser.^[139] In another study, aiming at improving the efficiency of crystalline silicon solar cell application (in which the absorption range of Yb³⁺ is not appropriate as it is covered by the crystalline silicon bandgap), Ho³⁺-doped Er₂O₃ thin films were successfully grown using a pre-doped (Er, Ho)(thd)₃ precursor that contained the two Ln metals at the required ratio.^[140]

Luminescent Ln³⁺ dopants are also useful for metal–oxide–semiconductor light-emitting devices (MOSLEDs), with application potential in optoelectronic devices, waveguides, and lasers.

Such Ln³⁺-doped MOSLEDs have attracted great attention for their outstandingly intense electroluminescence emission.^[143] The first ALD studies regarding the optoelectronic and waveguide applications are from 2004,^[144] and the research is still actively ongoing.^[145,146] For example, MOSLED structures with emission in the NIR range (977 nm) have been fabricated by depositing nanolaminates of Yb³⁺-doped Al₂O₃.^[147] However, for the MOSLED application, Er³⁺ with its emission maximum \approx 1530 nm is considered the best Ln dopant species (allowing the minimum loss window of optical telecommunications),^[148,149] and hence Er³⁺-doped thin films are increasingly investigated in ALD.^[150]

Finally, it should be mentioned that solid oxide fuel cell (SOFC) research could also benefit from the possibility of using rare earth elements as dopants in ALD. Most notably, thin films of yttria-stabilized zirconia (YSZ) (state-of-the-art solid-state electrolyte is SOFCs) were fabricated by including Y₂O₃ layers within ZrO₂ films; this was shown to enhance the fuel cell performance within the temperature range of 260–350 °C,^[151] while surface modification showed an increase in the maximum power density of the cell,^[152] and the ultra-thin ZrO₂:Y₂O₃ films fabricated with ALD were shown to be superior to bulk material regarding the electrical conductivity.^[153]

5. ALD Processes Based on Rare Earth Elements

The first ALD process involving a rare earth element as the main component was the Y(thd)₃ + ozone process for Y₂O₃ thin films

Precursor pulsing sequence

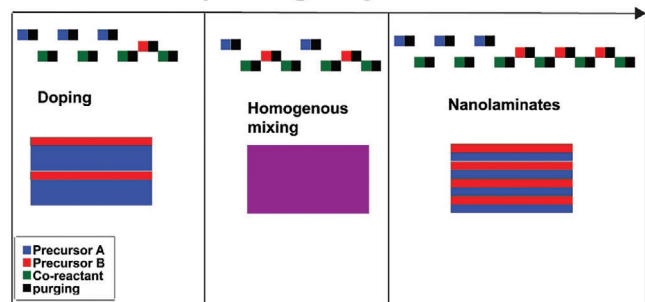


Figure 8. Different precursor dosing schemes in different ternary ALD processes for lightly-doped, homogeneously mixed, and nanolaminate materials.

reported in 1994.^[58] The films were deposited on several substrate materials including Si and soda lime glass. This was followed by a few La-based processes, not only for binary La_2O_3 films but also for ternary oxides with transition metals such as Ni and Co, and also for La_2S_3 .^[59,60,130,188] However, the real breakthrough came in the early 2000s when researchers started to explore rare earth element oxides (thanks to their high κ values) as potential gate insulators in MOSFETs to replace SiO_2 .^[189] This boosted the process development for R^{3+} -based binary oxides and also ternary oxides with Al or transition metals, and multi-layer films composed of R oxide(s), Al oxide, and/or transition metal oxide(s).

Initially, most of the ALD processes for the rare earth element compounds were based on the β -diketonate precursors, mainly thd complexes, in combination with ozone. In these processes, the deposition temperature plays a crucial role. Typically, the films grow amorphous until a threshold temperature is reached. For example, La_2O_3 films deposited below 300 °C are amorphous, while above 300 °C polycrystalline films with cubic symmetry are obtained. Orientation also depends on the deposition temperature such that in the temperature range of 300–350 °C the (222) diffraction peak is the strongest, while above 350 °C the (400) peak appears the strongest. Similar behavior is seen for La_2O_3 films grown on different substrate materials, and also for other $R(\text{thd})_3 + \text{O}_3$ processes.^[190]

The first non-oxide R -based ALD process was reported in 1998 for La_2S_3 films grown from $\text{La}(\text{thd})_3$ and H_2S . Also, fluoride processes have been developed using different fluoride sources as precursors, such as NH_4F and TiF_4 .^[63,133,191]

In general, binary ALD processes are straightforward to develop, while the ternary and quaternary processes require much more effort for optimization.^[192] Nevertheless, numerous ternary and quaternary R -based ALD processes with sufficient control over the metal composition have been successfully developed over the last two decades. In (Figure 8), we illustrate the use of the sequential pulsing of ALD to develop various ternary oxides and nanolaminates. These ternary oxide thin films have been investigated for their promising high- κ gate dielectric properties to replace SiO_2 in MOSFETs or to be used in hybrid floating gates in NAND flash,^[193,194] and also to obtain perovskite-structured compounds with unique electric and magnetic properties.^[195] Among the R s, lanthanum has been researched most widely as a con-

stituent of ternary oxides. Overall, a wide variety of ALD processes for ternary oxides have been developed in which the rare earth element is combined with another metal, including Al, Ti, Ni, Ga, W, Co, Mn, Fe, Hf, Y, Sc, Lu, and Li; a complete list is shown in Table 3.^[60,138,171,188,196–198] The most crucial issue in the deposition of ternary (and quaternary) thin films is to find the conditions to obtain reproducible and controllable ratio between the different elements using the supercycle concept.

Some examples of quaternary perovskites deposited by ALD are shown in (Figure 9). Especially the $(R,A)\text{BO}_3$ type perovskites have attracted continuous attention already for decades as they possess interesting electronic and magnetic properties. The pioneering ALD efforts to grow these perovskites were made in 2007, when Nilsen et al.^[199] developed an ALD process for $(\text{La},\text{Ca})\text{MnO}_3$ thin films based on $\text{La}(\text{thd})_3$, $\text{Ca}(\text{thd})_2$, $\text{Mn}(\text{thd})_3$, and O_3 precursors, having an eye on their interesting magnetic properties. However, the resulting films turned out to be Mn deficient and exhibited higher than aimed Ca content. Similar results were later obtained for the $(\text{La},\text{Sr})\text{FeO}_3$ films grown from $\text{La}(\text{thd})_3$, $\text{Ca}(\text{thd})_2$, $\text{Mn}(\text{thd})_3$, and O_3 ; these films were found to be Fe deficient and have higher than aimed Sr content.^[200] Later, relatively good compositional control has been reported for $(\text{La},\text{Sr})\text{CoO}_3$ ^[32] and $(\text{La},\text{Sr})\text{MnO}_3$ ^[151] that are potential SOFC cathode materials, and more recently also for $(\text{La},\text{Sr})\text{CuO}_4$ films (prototype high- T_c superconductor phase),^[201] and $\text{Gd}_{0.9}\text{Ca}_{0.1}\text{CoO}_3$.^[202] Promising results have also been reported for lithium solid electrolyte materials such as $\text{Li}_7\text{La}_3\text{Zr}_2\text{O}_{12}$ and $\text{Li}_{0.32}\text{La}_{0.30}\text{TiO}_2$, relevant for next-generation Li-ion battery technologies.^[29,146,196,200,203,204]

More recently, significant advances in the development of new ALD processes for R -fluorides have been rapidly made. Conventionally, the research on RF_3 thin films has been challenging due to safety concerns related to the commonly employed HF precursor, but recently safer fluoride precursors such as TiF_4 , NH_4F , and Nb_2F_5 have been successfully implemented in the process development of several RF_3 thin films (YF_3 , GdF_3 , LaF_3 , TbF_3 , and HoF_3) by ALD.^[63,133,134,191]

The deposition temperature affects the properties of RF_3 films heavily. In the case of GdF_3 from $\text{Gd}(\text{thd})_3$ and NH_4F , depositions at temperatures lower than 285 °C seem to contain some Gd_2O_3 as a secondary phase, while depositions at temperatures higher than 300 °C seem to contain the lowest amount of carbon impurities.^[63] Similarly, in the case of TbF_3 , deposition from $\text{Tb}(\text{thd})_3$ and TiF_4 at temperatures lower than 275 °C show high levels of impurities of C (4.3–5.3%), O (4.5–5.6%), and Ti (2.5–3.7%), while depositions at the higher temperatures (over 275 °C) show no Ti impurities, and C and O impurities of less than 1%.^[191]

The possibility to fabricate the thin films at relatively low temperature is important for many applications especially if temperature-sensitive substrates are used. ALD is in general considered superior compared to other gas-phase techniques which typically require significantly higher deposition temperatures. In this respect, plasma-enhanced (PE) ALD may provide further advantages; for the R -based materials, this was demonstrated by Fang et al. who fabricated GdN films from $\text{Gd}^{(\text{MeCp})_3}$ and N_2 plasma; this is actually the only ALD process reported so far for rare earth nitrides.^[62] Most of the PE-ALD processes for R -based materials are for oxides, and based on precursors previously

Table 3. ALD processes based on rare earth elements.

Material	Precursor 1	Precursor 2	Precursor 3	Precursor 4	GPC [Å]	T [°C]	Refs.
Sc_2O_3	$\text{Sc}(\text{thd})_3$	O_3			0.13	335–375	[125]
	$\text{Sc}(\text{Cp})_3$	H_2O			0.75	250–350	[125]
	$\text{Sc}(\text{iPr}^2\text{Cp})_3$	O_3			0.60–1.00	250–375	[207]
	$\text{Sc}(\text{iPr}^2\text{amd})_3$	H_2O			0.30	290	[104]
	$\text{Sc}(\text{MeCp})_3$	H_2O			0.65	300	[208–210]
	$\text{Sc}(\text{Me}^2\text{pz})(\text{MeCp})_2$	O_3			1.09–1.94	225,275	[211]
ScAlO_3	$\text{Sc}(\text{MeCp})_3$	TMA	H_2O		0.65	300	[194]
YScO_3	$\text{Y}(\text{thd})_3$	$\text{Sc}(\text{thd})_3$	O_3		0.18	335–350	[192]
	$\text{Y}(\text{MeCp})_3$	Cp_3Sc	H_2O		1.07	300	[192]
DyScO_3	$\text{Sc}(\text{thd})_3$	$\text{Dy}(\text{thd})_3$	O_3		0.43	350	[193]
Y_2O_3	$\text{Y}(\text{thd})_3$		O_3		0.22–0.23	250–300	[50,58,157,160,189,212–214]
	$\text{Y}(\text{thd})_3$	O_2 plasma			0.30	200–300	[158,159,206]
	$\text{Y}(\text{Cp})_3$		H_2O		1.20–1.30	200–400	[215]
	$\text{Y}(\text{MeCp})_3$		H_2O		1.00	250–325	[215]
	$\text{Y}(\text{EtCp})_3$		H_2O		1.70	200–400	[207,216]
	$\text{Y}(\text{iPr}^2\text{amd})_3$		H_2O		0.80	150–280	[100]
	$\text{Y}(\text{iPr}^2\text{Cp})_3$		O_3		1.70	245–300	[128]
	$\text{Y}(\text{iPr}^2\text{amd})\text{EtCp}_2$		H_2O		1.10	300–450	[217]
	$\text{Y}(\text{iPr}^2\text{amd})\text{EtCp}_2$		O_3		1.10	300–450	[217]
	$\text{Y}(\text{iPr}^2\text{amd})\text{EtCp}_2$		O_2		0.90	300–450	[217]
	$\text{Y}(\text{iPr}^2\text{amd})(\text{iPrCp})_2$		H_2O		0.40, 1.30	350–450	[117–119]
	$\text{Y}(\text{iPr}^2\text{amd})(\text{iPrCp})_2$		O_3		—	350	[118]
	$\text{Y}(\text{dpdmg})_3$		H_2O		1.10	175–250	[54]
	$\text{Y}(\text{Bu}^2\text{Cp})_3$		H_2O		1.40–1.70	230	[218]
	$\text{Y}(\text{iPr}^2\text{amd})\text{EtCp}_2$		H_2O		0.74	150–275	[120]
	$\text{Y}(\text{iPr}^2\text{amd})\text{EtCp}_2$	O_2 plasma			0.83	150–275	[120]
	$\text{Y}(\text{iPr}^2\text{amd})\text{EtCp}_2$	H_2O plasma			1.03	150–275	[120]
	$\text{Y}(\text{iPr}^2\text{famd})_3$		H_2O		1.36	150–325	[53]
	$\text{Y}(\text{tBu}^2\text{famd})_3$		H_2O		0.67	200–325	[114]
	$\text{Y}(\text{tBu}^2\text{Cp})_3$		H_2O		1.70	250	[219]
YMnO_3	$\text{Y}(\text{thd})_3$	$\text{Mn}(\text{thd})_3$	O_3		0.18–0.60	250–300	[220,221]
	$\text{Y}(\text{thd})_3$	$\text{Mn}(\text{thd})_3$	O_2		0.25–0.30	250	[222]
YAlO_3	$\text{Y}(\text{EtCp})_3$	TMA	H_2O		1.55	300	[223]
YVO_4	$\text{Y}(\text{thd})_3$	$\text{VO}(\text{thd})_2$	O_3		0.15–0.17	260–300	[141]
$\text{Y}_3\text{Ga}_5\text{O}_{12}$	$\text{Y}(\text{thd})_3$	Et_3Ga	O_3		0.23	350	[161]
$\text{Y}_2\text{O}_2\text{S}$	$\text{Y}(\text{thd})_3$	H_2S			—	350–450	[131]
$\text{Y}_2\text{O}_{3-x}\text{S}_x$	$\text{Y}(\text{MeCp})_3$	H_2O	H_2S		—	300	[184]
YF_3	$\text{Y}(\text{thd})_3$	TiF_4			1.10–1.70	225–325	[132]
La_2O_3	$\text{La}(\text{thd})_3$		O_3		0.36	180–425	[28,224–226]
	$\text{La}(\text{thd})_3$		H_2O		0.30–0.50	230–350	[227]
	$\text{La}(\text{thd})_3$ -DEMA		O_3		0.4	225–250	[228]
	$\text{La}(\text{iPrCp})_3$		H_2O		0.10	280–480	[229–232]
	$\text{La}(\text{iPrCp})_3$		O_3		0.30–0.60	150–250	[207,233]
	$\text{La}(\text{iPrCp})_3$	O_2 plasma			0.60	300–350	[230,234–238]
	$\text{La}(\text{Cp})_3$	H_2O			—	260	[225,239,240]
	$\text{La}(\text{Cp})_3$	O_2 plasma			0.50	150	[241]
	$\text{La}(\text{trmsa})_3$	H_2O			0.43	200–300	[242–245]
	$\text{La}(\text{iPr}^2\text{amd})_3$	H_2O			1.05	200–300	[129]
$[\text{La}(\text{iPr}^2\text{famd})_3]$	$[\text{La}(\text{iPr}^2\text{famd})_3]$	H_2O			1.70	200–250	[113]
	$[\text{La}(\text{iPr}^2\text{famd})_3]$	O_3			1.20–1.40	200–250	[113]

(Continued)

Table 3. (Continued)

Material	Precursor 1	Precursor 2	Precursor 3	Precursor 4	GPC [Å]	T [°C]	Refs.
	La(ⁱ Pr ₂ famd) ₃	O ₂			0.40	300	[246]
	La(ⁱ Pr ₂ amd)(ⁱ PrCp) ₂	H ₂ O			1.20–3.00	200–300	[116]
	La(ⁱ Pr ₂ amd)(ⁱ PrCp) ₂	O ₃			0.60–2.10	200–325	[116]
	La(ⁱ Pr ₂ amd)(ⁱ PrCp) ₂	H ₂ O + O ₃			0.70–1.80	200–325	[116]
	La(ⁱ Pr ₂ amd)(ⁱ PrCp) ₂	EtOH			0.50–1.70	200–325	[116]
LaAlO ₃	La(thd) ₃	Al(acac) ₃	O ₃		0.36–0.39	325–400	[247]
	La(thd) ₃	TMA	H ₂ O		0.55	270	[248]
	La(thd) ₃	TMA	O ₃		0.64	250	[249]
	La(tmsa) ₃	TMA	H ₂ O		0.58	225–250	[244]
	La(ⁱ Pr ₂ amd) ₃	TMA	H ₂ O		0.80	300–330	[250]
	La(ⁱ Pr ₂ famd) ₃	TMA	H ₂ O		2.80	300–330	[251]
	La(ⁱ PrCp) ₃	TMA	H ₂ O		0.12	300	[252,253]
	LaAl(O ⁱ Pr) ₆ (ⁱ PrOH)] ₂	H ₂ O			0.10–0.50	160–300	[138]
LaNiO ₃	La(thd) ₃	Ni(thd) ₂	O ₃		0.08–0.26	215–400	[60]
	La(thd) ₃	Ni(acac) ₂	O ₃		0.31	225	[195,254]
LaCoO ₃	La(thd) ₃	Co(thd) ₂	O ₃		0.35	200–400	[188]
LaMnO ₃	La(thd) ₃	Mn(thd) ₂	O ₃		0.10–0.23	250–325	[196,221]
LaGaO ₃	La(thd) ₃	Ga(acac) ₃	O ₃		0.38	325–400	[197]
LaFeO ₃	La(thd) ₃	Fe(thd) ₃	O ₃		0.20–0.30	200–360	[200]
LaLuO ₃	La(thd) ₃	Lu(thd) ₃	O ₃			300	[33]
	La(ⁱ Pr ₂ amd) ₃	Lu(^E t famd) ₃	H ₂ O		1.20	300	[33]
LaScO ₃	La(ⁱ Pr ₂ amd) ₃	Sc(^E t amd) ₃	H ₂ O		1.10	300	[33]
LaYO ₃	La(ⁱ Pr ₂ amd) ₃	Y(ⁱ Pr amd) ₃	H ₂ O		0.80	280	[33]
HfLaO _x	La(ⁱ PrCp) ₃	TEMA-Hf	H ₂ O		1.40	300	[229]
	La(ⁱ PrCp) ₃	TEMA-Hf	O ₃			NA	[207]
	La(ⁱ PrCp) ₃	TEMA-Hf	O ₂ plasma		0.50	225,300–350	[234]
	La(ⁱ Pr ₂ famd) ₃	TEMA-Hf	O ₃			—	[255]
LiLaO ₂	Li(thd)	La(thd) ₃	O ₃		0.20–0.30	225	[256]
LaWO ₄	La(thd) ₃	W(^t BuN) ₂ (Me ₂ N) ₂	O ₃	H ₂ O	0.48–0.58	250–375	[198]
LaPO ₄	La(thd) ₃	TMPO	H ₂ O	O ₃	0.78	275	[257]
LaCaPO ₄	La(thd) ₃	Ca(thd) ₂	TMPO	H ₂ O /O ₃	0.78	275	[257]
La ₂ CuO ₄	La(thd) ₃	Cu(acac) ₂	O ₃		0.40	210–250	[258]
LaVO ₄	La(thd) ₃	VO(acac) ₂			—	270	[259]
La _x Zr _{1-x} O _{2-δ}	La(ⁱ PrCp) ₃	(^M eCp) ₂ ZrMe(OMe)	H ₂ O		—	300	[260,261]
	La(thd) ₃	(^M eCp) ₂ ZrMe(OMe)	O ₃		—	300	[262]
	La(tmsa) ₃	Zr[N(CH ₂ CH ₃)] ₄	H ₂ O		0.58–0.72	250	[263]
Li _{0.32} La _{0.30} TiO ₂	La(thd) ₃	O ₃	TiCl ₄ / LiO ^t Bu	H ₂ O	0.15–0.35	225	[204]
Li ₂ La ₃ Zr ₂ O ₁₂	LiO ^t Bu	[La(ⁱ PrFamnd) ₃]	TDMAZ	O ₃	0.80	225	[203]
La _{1-x} Sr _x FeO ₃	La(thd) ₃	Sr(thd) ₂	Fe(thd) ₃	O ₃	0.20–0.30	260	[200]
La _{1-x} Sr _x MnO ₃	La(^M eCp) ₃	Sr ⁿ ^M eCp ₂	Mn ^M eCp ₂	H ₂ O	5.00	300	[151]
La _{1-x} Ca _x MnO ₃	La(thd) ₃	Ca(thd) ₂	Mn(thd) ₃	O ₃	0.15–0.40	235–285	[199]
(La,Sr)CoO _{3-δ}	La(thd) ₃	Sr(thd) ₂	Co(acac) ₃	O ₃	0.50	250–310	[32]
La _{2-x} Sr _x CuO _{4-y}	La(thd) ₃	Cu(acac) ₂	Sr(thd) ₂	O ₃	0.40	225	[201]
LaNi _x Cu _{1-x} O ₃	La(thd) ₃	Ni(acac) ₂	Cu(acac) ₂	O ₃	—	225	[205]
LaF ₃	La(thd) ₃	TiF ₄			2.00–5.00	225–350	[133]
	La(thd) ₃	O ₃	Hfac		0.49	250–300	[264]
La ₂ S ₃	La(thd) ₃	H ₂ S			0.15	360–410	[130]
CeO ₂	Ce(thd) ₄	O ₃			0.32	175–375	[182,265–268]
	Ce(thd) ₃ phen	O ₃			0.42	225–350	[265]
	Ce(mmp) ₄	O ₂ plasma			—	150–300	[85]

(Continued)

Table 3. (Continued)

Material	Precursor 1	Precursor 2	Precursor 3	Precursor 4	GPC [Å]	T [°C]	Refs.
	Ce(ⁱ PrCp) ₃	O ₂ plasma			0.35	250	[269]
	Ce(ⁱ PrCp) ₃	H ₂ O			0.20	250	[270]
	Ce(ⁱ Pr ² amd)(ⁱ PrCp) ₂	H ₂ O			1.90	240	[115]
	Ce(ⁱ Pr ² amd) ₃	O ₃			2.80	210–270	[105]
	Ce(dpdmg) ₃	H ₂ O			2.10	160	[124]
	Ce(ⁱ Pr ² famd)(ⁱ PrCp) ₂	H ₂ O			1.50	245	[271]
CeO ₂ , Y ₂ O ₃	Ce(thd) ₄	Y(thd) ₃	O ₃		0.41–0.53	300	[136, 182]
CeGdO ₃	Ce(thd) ₄	Gd(thd) ₃	O _{3k}		0.32	250	[272]
CeVO ₄	Ce(thd) ₄	VO(acac) ₂			—	270	[259]
CeFeO _x	Ce(thd) ₄	Fe(CP) ₂			—	270	[273]
CeMnO ₃	Ce(thd) ₄	Mn(thd) ₃			—	270	[274]
Pr ₂ O ₃	Pr(tmsa) ₃	H ₂ O			0.15–2.90	200–400	[94]
	Pr(mmp) ₃	H ₂ O			0.10–0.70	200–350	[96]
	Pr(^E CP) ₃	H ₂ O			0.70	130	[275]
	Pr(ⁱ Pr ² amd)(ⁱ PrCp) ₂	H ₂ O			1.47–1.66	200–300	[118]
Pr _x Al _{2-x} O ₃	Pr(ⁱ Pr ² amd) ₃	TMA	H ₂ O		0.8–1.0	295	[102]
	[PrAl(OPr) ₆ (Pr ⁱ OH)] ₂	H ₂ O			—	180–350	[276]
	Pr(ⁱ PrCp) ₃	TMA	H ₂ O		1.70	250–350	[277]
Nd ₂ O ₃	Nd(thd) ₃	O ₃			0.44–0.45	310	[82, 84, 140, 214, 278]
NdAlO ₃	Nd(thd) ₃	O ₃	TMA	H ₂ O	0.53	300	[126]
	[NdAl(O ⁱ Pr) ₆ (Pr ⁱ OH)] ₂	H ₂ O			—	180–350	[276]
NdNiO ₃	Nd(ⁱ PrCp) ₃	Ni(^t Bu ₂ amd) ₂	O ₃		0.36	160	[279]
Sm ₂ O ₃	Sm(thd) ₃	O ₃			0.36	300	[82]
SmMnO ₃	Sm(thd) ₃	Mn(thd) ₂	O ₃		0.23	275	[221]
Eu ₂ O ₃	Eu(thd) ₃	O ₃			73	0.32	[82, 280–284]
Eu _x Ti _y O _z	Eu(thd) ₃	O ₃	TiCl ₄	H ₂ O	0.38–0.45	300	[285]
Eu _x Ti _y PO _z	Eu(thd) ₃	O ₃	TiCl ₄ +H ₂ O	Me ₃ PO ₄	0.80–1.00	300	[286]
Gd ₂ O ₃	Gd(thd) ₃	O ₃			0.31	300	[82]
	Gd(^M CP) ₃	H ₂ O			1.00–3.20	175–300	[83]
	Gd(^R CP) ₃	H ₂ O			1.00–3.20		[287, 288]
	Gd(mmp) ₃	H ₂ O			0.20–1.00	200–300	[96]
	Gd(dpdmg) ₃	H ₂ O			1.00–1.10	175–350	[107, 109, 289, 290]
	Gd(^t Bu ² amd) ₃	H ₂ O			0.26–0.49	350–400	[86, 97, 291, 292]
	Gd(ⁱ PrCp) ₃	O ₂ plasma			1.40	250	[293]
	Gd(ⁱ PrCp) ₃	H ₂ O			0.80	250	[208, 209]
	Gd(ⁱ PrCp) ₃	O ₃			0.20	250	[294]
	Gd(ⁱ Pr ² amd)(ⁱ PrCp) ₂	H ₂ O			1.16–1.38	200–250	[118]
GdAlO ₃	Gd(ⁱ PrCp) ₃	TMA	O ₃		1.75–2.75	200–350	[295]
	Gd(ⁱ PrCp) ₃	TMA	H ₂ O		4.50–5.00	200–350	[295]
ZrO ₂ -Gd ₂ O ₃	Zr(^M CP) ₂ Me(OMe)	Gd(thd) ₃	O ₃		0.39–0.53	300	[296]
GdScO ₃	Gd(ⁱ Pr ² amd) ₃	Sc(^E t ² amd) ₃	H ₂ O		2.00	310	[103]
	Gd(thd) ₃	Sc(thd) ₃	O ₃		0.21	300	[297]
	Gd(ⁱ PrCp) ₃	Sc(^M eCP) ₃	H ₂ O		2.20	300	[194, 209]
GdFeO ₃	GdFeO(^t Bu) ₆ (C ₅ H ₅ N) ₂	O ₃			0.20–0.30	200	[298]
GdCoO ₃	Gd(thd) ₃	Co(thd) ₂	O ₃		0.24	300	[202]
Gd ₃ Ga ₅ O ₁₂	Gd(thd) ₃	TEGa	O ₃		0.19	350	[185]
Gd _{0.9} Ca _{0.1} CoO ₃	Gd(thd) ₃	Co(thd) ₂	Ca(thd) ₂	O ₃	0.30	300	[202]
GdN	Gd(^M eCP) ₃	N ₂ plasma			0.33	150–300	[62]
GdF ₃	Gd(thd) ₃	NH ₄ F			0.26	300	[63]
Tb ₂ O ₃ -Al ₂ O ₃	Tb(thd) ₃	TMA	O ₃		—	350	[299]

(Continued)

Table 3. (Continued)

Material	Precursor 1	Precursor 2	Precursor 3	Precursor 4	GPC [Å]	T [°C]	Refs.
TbMnO ₃	Tb(thd) ₃	Mn(thd) ₂	O ₃		0.18	250–325	[221]
TbScO ₃	Tb(thd) ₃	Sc(thd) ₃	O ₃		0.40	300	[300]
TbF ₃	Tb(thd) ₃	TiF ₄			0.75	175–350	[191]
Dy ₂ O ₃	Dy(thd) ₃	O ₃			0.31	300	[82,180]
	Dy(dpdmg) ₃	H ₂ O			1.00	200–350	[107,289]
	Dy(ⁱ Pr ₂ amd)(ⁱ PrCp) ₂	O ₂ plasma			0.30	140–230	[301]
	Dy(ⁱ Pr ₂ amd)(ⁱ PrCp) ₂	H ₂ O			1.16–1.38	300–350	[118]
	Dy(ⁱ Pr ₂ amd)(ⁱ PrCp) ₂	O ₃			—	200–350	[118]
Ho ₂ O ₃	Ho(thd) ₃	O ₃			0.25	300	[82]
HoF ₃	Ho(thd) ₃	NbF ₅			1.00	250–275	[134]
Er ₂ O ₃	Er(thd) ₃	O ₃			0.20–0.25	250–375	[82,84,140,214,278]
	Er(thd) ₃	O ₂ plasma			0.50	200–300	[302]
	Er(^M eCp) ₃	H ₂ O			1.50	250–350	[86,278]
	Er(^M eCp) ₃	O ₃			0.12	170–330	[87,207]
	Erbitel 12	O ₃			0.20–0.40	175–300	[207]
	Er(^t Bu ₂ amd) ₃	O ₃			0.37–0.55	225–300	[101]
	Er(dpdmg) ₃	H ₂ O			1.10	150–275	[108]
	Er(ⁱ Pr ₂ amd)(^M eCp) ₂	H ₂ O			0.50	180	[301]
	Er(ⁱ Pr ₂ amd)(^M eCp) ₂	O ₂ plasma			0.70	180	[301]
	Er(ⁱ Pr ₂ amd)(^M eCp) ₂	H ₂ O			1.10–1.20	225–275	[78]
	Er(ⁱ Pr ₂ amd)(^M eCp) ₂	O ₃			0.20–1.0	200–325	[78]
	Er(ⁱ PrCp) ₃	H ₂ O			0.80–1.20	200–300	[78]
	Er(ⁱ PrCp) ₃	O ₃			0.30–0.80	200–300	[78]
	Er(ⁿ BuCp) ₃	H ₂ O			1.20	250–325	[78]
	Er(ⁿ BuCp) ₃	O ₃			0.40–0.80	225–350	[78]
Er _{1-x} Ti _x O _y	Er(^M eCp) ₃	TDEAT	O ₃		0.5–10.64	175–275	[303]
ZrO ₂ ·Er ₂ O ₃	Zr(^M eCp) ₂ Me(OMe)	Er(thd) ₃	O ₃		0.20	350	[34]
(Er,Ga) ₂ O ₃	Er(thd) ₃	Ga(acac) ₃	O ₃		0.25–0.28	350	[304]
	Er(^M eCp) ₃	Ga ₂ (NMe ₂) ₆	H ₂ O		0.95–1.00	250	[304]
ErFeO ₃	Er(thd) ₃	Fe(thd) ₃	O ₃		1.00	280–300	[305]
Tm ₂ O ₃	Tm(thd) ₃	O ₃			0.22	300	[82,306,307]
	Tm(Cp) ₃	H ₂ O			1.50	200–300	[308]
Yb ₂ O ₃	Yb(thd) ₃	O ₃			0.15–0.2	250–400	[139,148,309]
	Yb(^M eCp) ₃	H ₂ O			1.00	180–375	[207]
Yb ₃ Al ₅ O ₁₂	Yb(thd) ₃	TMA	O ₃		0.20	350	[149]
Yb _x Ti _y O _z	Yb(thd) ₃	O ₃	TiCl ₄	H ₂ O	0.36–0.37	300	[293]
YbMnO ₃	Yb(thd) ₃	Mn(thd) ₂	O ₃		0.18	275–300	[221]
YbVO ₄	Yb(thd) ₃	VO(thd) ₂	O ₃		0.08–0.23	240	[310]
Lu ₂ O ₃	Lu(^{Si} Me ₃ Cp) ₂ Cl	H ₂ O			0.25	360–370	[311,312]
	Lu(ⁱ PrCp) ₃	H ₂ O			—	330	[80]
LuMnO ₃	Lu(thd) ₃	Mn(thd) ₃	O ₃		0.18	275–300	[221]
LuAlO ₃	Lu(thd) ₃	TMA	O ₃		0.35	300	[313]
	Lu(ⁱ PrCp) ₃	TDEAA	O ₃		1.30	250	[135]
	Lu(ⁱ PrCp) ₃	TDEAA	H ₂ O		1.30	250	[135]
Lu ₃ Al ₅ O ₁₂	Lu(thd) ₃	TMA	O ₃		0.19	350	[150]
Lu	Lu(thd) ₃	O ₃			0.30	230	[314]
LuSi _{1.5} O ₅	Lu(tmsa) ₃	H ₂ O / O ₃			0.60–4.3	280–380	[82,315]
Lu ₃ Ga ₅ O ₁₂	Lu(thd) ₃	Ga(C ₂ H ₅) ₃	O ₃		0.20	350	[316]

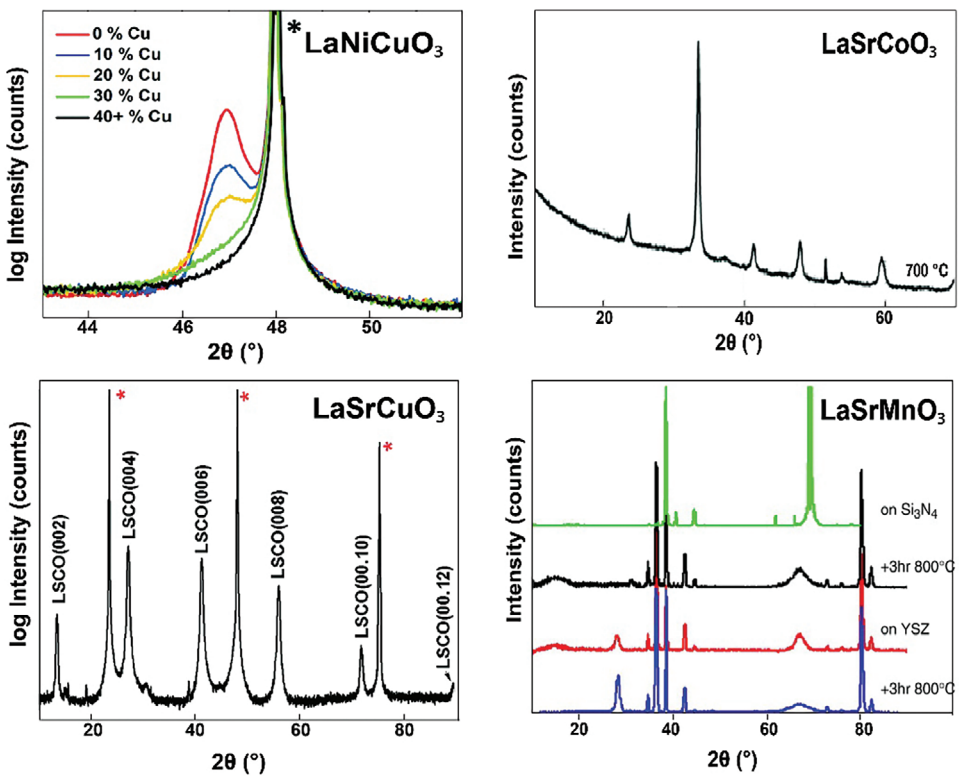


Figure 9. XRD patterns for various R -based quaternary oxide thin films deposited by ALD: $\text{La}(\text{Ni},\text{Cu})\text{O}_3$,^[205] (Reproduced with permission, 2020, Royal Society of Chemistry.) $(\text{La},\text{Sr})\text{CoO}_3$,^[32] (Reproduced with permission, 2015, Royal Society of Chemistry.) $(\text{La},\text{Sr})\text{CuO}_3$,^[201] (Reproduced with permission, 2018, Royal Society of Chemistry.) and $(\text{La},\text{Sr})\text{MnO}_3$.^[151] Reproduced with permission, 2008, Elsevier).

experimented in the context of thermal ALD. One of the advantages of PE-ALD is the ability to use $R(\text{thd})_3$ precursors with O_2 or H_2O plasma, while those co-reactants are not reactive enough toward R^{3+} β -diketonate precursors under thermal ALD conditions.^[206] Also importantly, the PE-ALD $R(\text{thd})_3 + \text{plasma-O}_2$ processes yield higher growth rates compared to thermal-ALD $R(\text{thd})_3 + \text{O}_3$ processes, as is clearly seen in Table 3 which summarizes all the ALD processes developed for R^{3+} materials.

6. ALD/MLD Processes with Rare Earth Elements

The first ALD/MLD study involving rare earth elements was reported in 2015, for flexible photoluminescent Eu-PDA (europium 1,4-pyridine dicarboxylate) thin films.^[43] This was soon followed by another report in which europium was combined with several different organic components.^[317] In (Figure 10), the molecular structures of all the organic precursors so far employed in ALD/MLD experiments in combination with rare earth elements are shown. This figure also shows the acronyms used for these precursors, together with the heating temperatures employed in ALD/MLD depositions for their evaporation.

Most of the organic precursors are solids of somewhat bigger organic molecules with low vapor pressures, meaning that relatively high heating temperatures are required for their vaporization. Hence, in a majority of the ALD/MLD processes of R -organic thin films, the deposition temperature has been relatively high, varying between 145 and 420 °C. This may be an

issue, considering the potential future industrial-scale applications, in which liquid precursors are typically favored over solid ones. However, there are also examples of processes working at relatively low temperature, allowing the growth of R -organic thin films on flexible substrates such as polymer sheets and yarns.^[43,318]

The low precursor volatility may potentially lead to conformality issues on large surface area substrates. A plausible solution to overcome this issue is to increase the organic precursor sublimation temperature.^[43] The drawback is that at higher deposition temperatures (needed to match the higher precursor evaporation temperature) the growth rates are lower; another potential issue is the increased probability of precursor decomposition. There are no dedicated conformality studies reported for R -organic thin films. However, the fact that red PL emission from the Eu-HQA (HQA = 2-hydroxyquinoline-4-carboxylic acid) films deposited on nanoplasmonic structures was highly homogeneous could be taken as an indication of conformal film growth.^[55]

Trivalent europium is known for its intense red luminescence emission, and in several ALD/MLD investigations, the goal has been to manipulate the absorption and/or emission properties of Eu^{3+} through the choice of the organic component. For example, by increasing the number of aromatic rings in the backbone from the single ring as in TPA (terephthalic acid or 1,4-benzene dicarboxylic acid) to two rings as in NDA (2,6-naphthalene dicarboxylic acid) and ADA (9,10-anthracene dicarboxylic acid) the emission wavelength was red-shifted, but at the cost of weakening

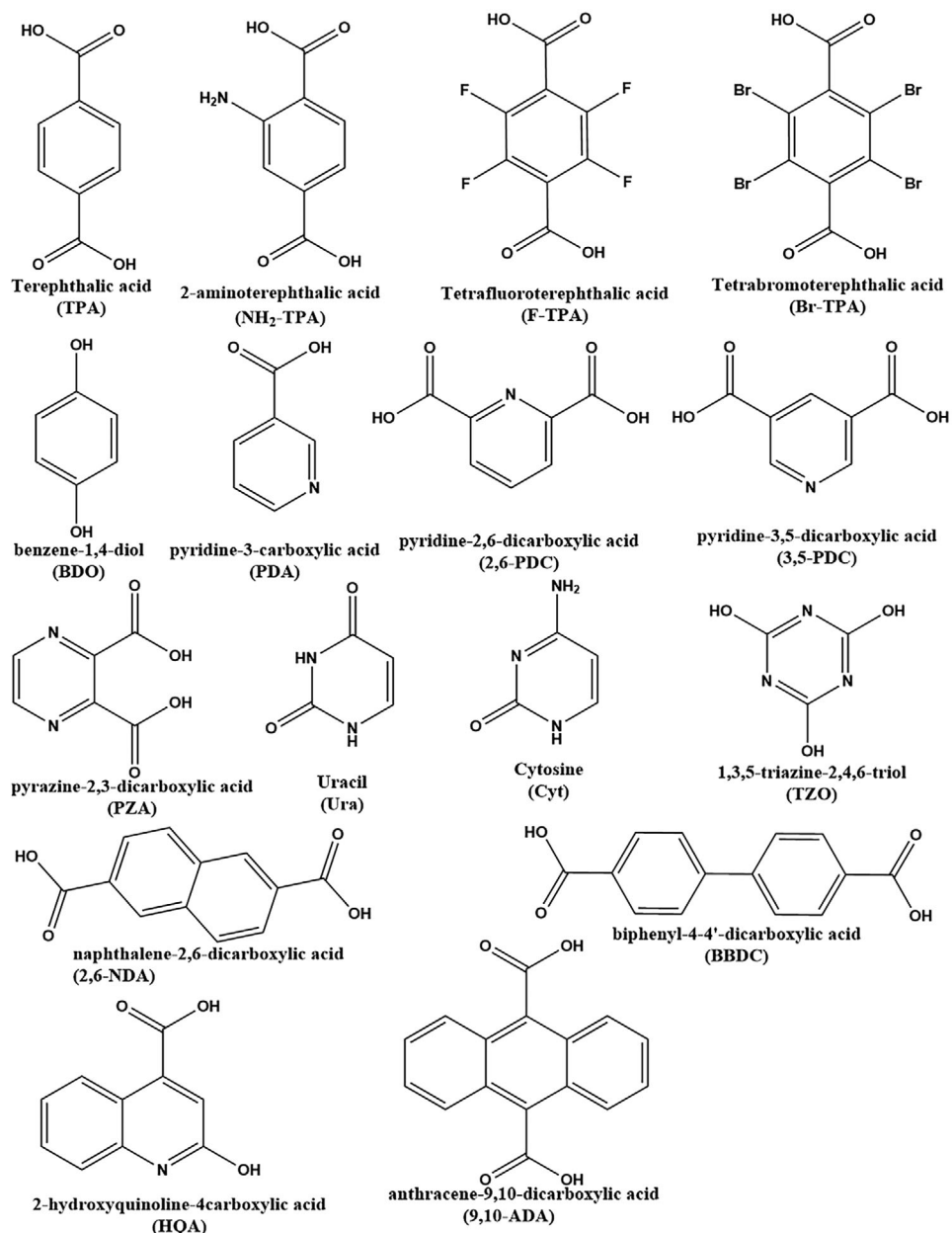


Figure 10. Organic molecules used as precursors in ALD/MLD processes in combination with rare earth elements.

emission intensity. On the other hand, by diluting the europium content with non-photoactive yttrium the emission intensity could be significantly enhanced for (Eu_{0.12}Y_{0.88})-TPA thin films.^[319]

Indeed, the ALD/MLD approach allows—like its parent ALD technique—the combination of several different *R* species into the same thin-film material; through such efforts white light emissive thin films consisting of red, green, and blue emitting Ln³⁺ species were recently realized.^[320]

Another important target in the ALD/MLD research has been in the up-converting Ln-organic thin films, such as (Y,Yb,Er)-pyrazine,^[321] and (Yb,Er)-IR-806 films.^[322] Luminescent Ln-organic thin films realized through ALD/MLD have several po-

tential advantages compared to the purely inorganic Ln-based thin films grown with ALD, as: i) the organic component is likely to enhance the mechanical properties of the films,^[323] ii) organic linkers are anticipated to provide proper spacing between the Ln³⁺ species such that the unwanted concentration quenching can be minimized/avoided, iii) organic linkers may also act as a sensitizer for the Ln³⁺ luminescence,^[324] and most excitingly iv) the excitation wavelength range can be tailored by the choice of the organic linker.

An illustrative example of the excitation wavelength engineering through the choice of the organic precursor is shown for Eu-organic thin films in (Figure 11). Among the four different Eu-organic thin-film materials, Eu-TPA shows a strong excitation

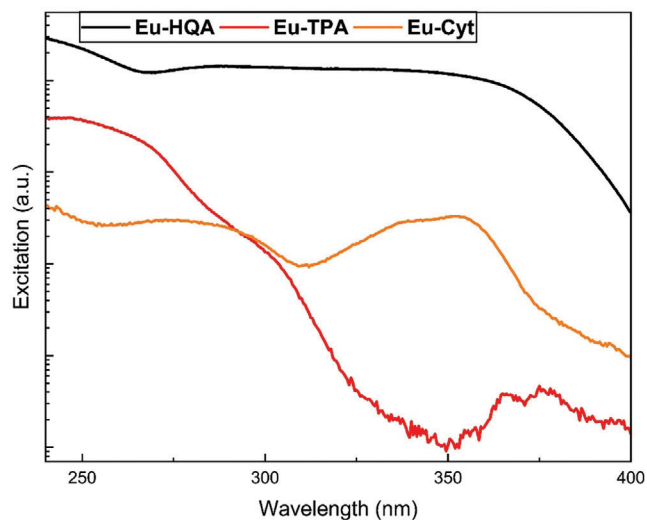


Figure 11. Excitation spectra of Eu-HQA, Eu-TPA, and Eu-Cyt thin films on silicon substrates, illustrating the effect of the chosen organic precursor on the properties of the ALD/MLD deposited thin films.^[55,318]

band that peaks around $\lambda \approx 250$ nm. By replacing TPA with other organics the excitation wavelength could be effectively shifted to higher wavelengths even up to visible range, i.e. to $\lambda \approx 270$ nm for PDA (pyridine dicarboxylic acid),^[317] to $\lambda \approx 350$ nm for Cyt (cytosine),^[318] and to cover the entire 200–400 nm range for HQA (2-hydroxyquinoline-4-carboxylic acid).^[55]

While most of the ALD/MLD processes developed so far for different R^{3+} -organic thin films have been based on the well-established $R(\text{thd})_3$ precursors (Table 4), attempts to deploy other more reactive rare earth element precursors have shown significantly higher growth rates, with GPC values reaching 5.4 Å in case of Ce-TPA and 6.4 Å for Er-TPA; in these processes $\text{Ce}(\text{dpdmg})_3$ and $\text{Er}(\text{dpdmg})_3$ were used and steric hindrance was assumed to be behind the higher GPC values. Most of the R^{3+} -organic thin films have been amorphous, but there are two significant exceptions. First, the La-TPA films grown from $\text{La}(\text{thd})_3$ and TPA were found to be in-situ crystalline.^[325] Secondly, their neodymium counterparts, i.e., the Nd-TPA films were first amorphous but were crystallized upon absorbing water as guest molecules in the structure.^[326]

7. Application Prospects of R-Based Thin Films

Rare earth element-based thin films fabricated through ALD or ALD/MLD have been recognized as highly promising candidates for a wide range of applications, such as gate dielectrics, optical thermometry, waveguides, bio-imaging, and bio-detection. This chapter highlights some of these potential application areas.

7.1. Gate Dielectrics in Microelectronics

With the progressively tightening requirements set for the so-called gate oxide thin-film layers in the continuously miniaturized integrated circuits,^[329] it became clear already more than a decade ago that the traditionally utilized SiO_2 layers did not suffice anymore once the layer thickness was radically decreased,

Table 4. ALD/MLD processes based on rare earth elements.

Material	Precursor 1	Precursor 2	GPC [Å]	T [°C]	Refs.
Y-2,6NDC	$\text{Y}(\text{thd})_3$	2,6NDA	2.0	260	[327]
(Y,Yb,Er)-2,3PZA	$(\text{Y},\text{Yb},\text{Er})(\text{thd})_3$	2,3PZA	3.4	160-280	[321]
La-TPA	$\text{Nd}(\text{thd})_3$	TPA	3.2	200	[325]
Ce-TPA	$\text{Ce}(\text{dpdmg})_3$	TPA	5.4	200	[61]
Nd-TPA	$\text{Nd}(\text{thd})_3$	TPA	3.2	200	[326]
Eu-TPA	$\text{Eu}(\text{thd})_3$	TPA	2.5-3.2	190-240	[317-319]
Eu-2,6PDC	$\text{Eu}(\text{thd})_3$	2,6PDC	2.0-1.3	240-340	[317]
Eu-3,5PDC	$\text{Eu}(\text{thd})_3$	3,5PDC	3.0-2.0	240-340	[317]
Eu-2,6NDC	$\text{Eu}(\text{thd})_3$	2,6NDA	3.0	220	[319]
Eu-9,10ADC	$\text{Eu}(\text{thd})_3$	9,10ADA	3.0	250	[319]
Eu-NH2TP	$\text{Eu}(\text{thd})_3$	NH2-TPA	NG	180-250	[328]
Tb-TP	$\text{Tb}(\text{thd})_3$	TPA	2.5	250	[327]
Tb-bdo	$\text{Tb}(\text{thd})_3$	BDO	1.2	175	[327]
Tb-FTP	$\text{Tb}(\text{thd})_3$	F-TPA	2.4	250	[327]
Tb-BrTP	$\text{Tb}(\text{thd})_3$	Br-TPA	2.7	250	[327]
Tb-NH2TP	$\text{Tb}(\text{thd})_3$	NH2-TPA	2.7	250	[327]
Tb-bpdc	$\text{Tb}(\text{thd})_3$	BPDCA	2.6	275	[327]
Tb-2,6NDC	$\text{Tb}(\text{thd})_3$	2,6-NDA	2.7	250	[327]
Er-3,5PDC	$\text{Er}(\text{dpdmg})_3$	3,5PDC	6.4	245-280	[110]
(Yb,Er)-IR806	$\text{Yb,Er}(\text{dpdmg})_3$	IR806	2.50	250-280	[322]
La,(Er,Tb,Eu)-TP	$\text{Ln}(\text{thd})_3$	TPA	3.20	190	[320]
Eu-PDA	$\text{Eu}(\text{thd})_3$	3-PDA	1.7	180	[318]
Eu-PZA	$\text{Eu}(\text{thd})_3$	2,3-PZA	3.5	180	[318]
Eu-Ura	$\text{Eu}(\text{thd})_3$	Uracil	2.1	250	[318]
Eu-Cyt	$\text{Eu}(\text{thd})_3$	Cytosine	1.5	250	[318]
Eu-TZO	$\text{Eu}(\text{thd})_3$	TZO	2.1	250	[318]
Eu-HQA	$\text{Eu}(\text{thd})_3$	HQA	7.3	210	[55]

due to the strongly increased current leakages caused by the direct tunneling of electrons.^[330] This progress in device miniaturization led to the need to develop new high-dielectric-constant (κ) materials and fabrication technologies enabling the decrease of the tunneling current in the ultrathin high- κ dielectric oxide layers. Moreover, a high band offset was required for the next-generation gate dielectric oxide thin films.^[331]

Rare earth oxides were considered very promising dielectrics to replace SiO_2 , thanks to their high- κ values, relatively large bandgap values, and excellent thermal and chemical stability.^[17] In particular, $R_2\text{O}_3$ thin films have shown interesting electrical properties.^[82] The ALD process used has an impact on the properties of these thin films; for example, $\text{La}(\text{OH})_3$ tends to form when water is employed as the oxygen source which may increase the current leakage, a problem that may be solved by choosing O_3 as the source of oxygen.^[113] Similarly, using plasma-enhanced ALD of $\text{La}(\text{iPrCp})_3$ and O_2 -plasma has led to better electrical properties of La_2O_3 thin films compared to films produced through thermal ALD from the same La precursor with water.^[230]

ALD also allows the fabrication of high-quality ternary oxides in which La is combined with another metal. An interesting example is the $(\text{La},\text{Al})_2\text{O}_3$ films reported by Fei et al.; the aluminum addition increased the dielectric constant (≈ 5) and equivalent oxide thickness (EOT = thickness of SiO_2 layer that would offer an

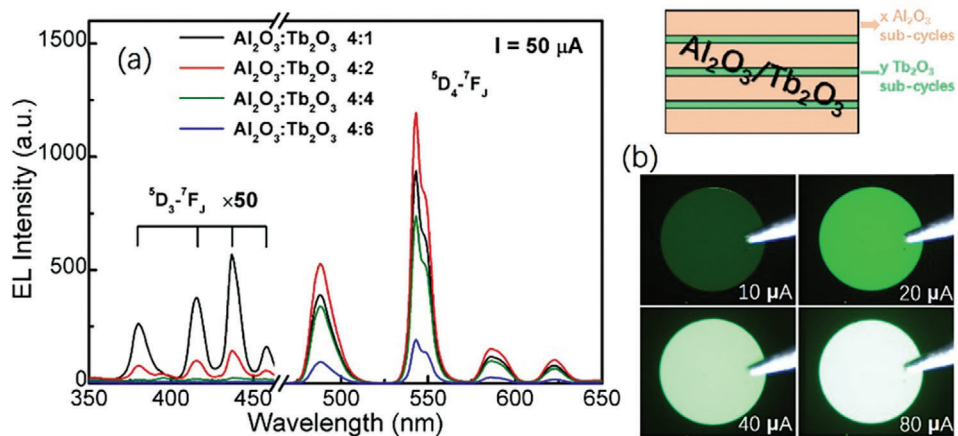


Figure 12. Green Tb^{3+} EL emission from different ALD-grown nanolaminates consisting of Al_2O_3 and Tb_2O_3 layers, relevant for use in luminescent displays. Republished with permission from Ref. [299], 2018, Optica publishing group.

equivalent electrical performance ignoring the current leakage; $\approx 8.3 \text{ nm}$) values of La_2O_3 thin films to $\kappa \approx 17$ and EOT ≈ 3.9 for the $(\text{La},\text{Al})_2\text{O}_3$ films grown with the 1:1 ratio of La and Al precursor pulses. By increasing La:Al pulse ratio enhanced the electrical performance further, for the 2:1 films to $\kappa \approx 21.9$ and EOT $\approx 3.4 \text{ nm}$, and for the 3:1 films to $\kappa \approx 24.9$ and EOT $\approx 2.9 \text{ nm}$.^[253] The ALD research on dielectric ternary oxides includes—besides lanthanum—also many other rare earth elements. For example, GdScO_3 films showed a dielectric constant of ≈ 21.5 and EOT $\approx 1 \text{ nm}$.^[103] Also, for the $(\text{Pr}_{1.15}\text{Al}_{0.85})\text{O}_3$ films an impressive EOT value of $\approx 1.5 \text{ nm}$ and dielectric constant of ≈ 17.7 were reported.^[102]

7.2. Luminescence Applications

The most characteristic luminescence properties of Ln^{3+} ions arise from the well-defined sharp-line transitions within their partially filled 4f orbitals; the spatially extended 5s and 5p orbitals offer shielding to the core 4f electrons which makes the emission independent of the coordination environment or the host material.^[17] The 4f–4f transitions are parity forbidden, which means that the excitation efficiency is low; another consequence is the long excited-state lifetime up to milliseconds. Some of the lanthanides show also luminescence arising from parity-allowed 4f–5d transitions; these transitions show short excited-state lifetimes of nanosecond range and they can be heavily affected by the host environment, which allows emission tunability.^[27] Most of the applications are based on the 4f–4f transitions of Eu^{3+} and Tb^{3+} yielding visible light emissions and those of Er^{3+} and Nd^{3+} with emission in the NIR range, or the 4f–5d transitions of Ce^{3+} , Pr^{3+} , and Eu^{2+} .^[332] The excitation is made either through electric current (electroluminescence; EL) or light (photoluminescence; PL).

7.2.1. Electroluminescent Displays

The first prospective application area of the ALD-grown Ln-doped thin films was seen in thin-film electroluminescent (TFEL) devices, first highlighted in 1992 for Tb^{3+} -doped ZnS thin films.^[22]

More recently, besides the metal sulfide matrices, other inorganic matrices have been highlighted as well, with excellent chemical and physical stabilities even under high temperatures.^[142,333] The TEFL-based screens have established their position in the screens industry over more than 40 years. (Figure 12) shows a typical electroluminescence by Tb^{3+} that can be used in transparent displays, where doping Y_2O_3 with Eu^{3+} shows intense red emission upon electroluminescence.^[146]

Another strategy to apply ALD for TEFL is using nanolaminates of Tb_2O_3 and Al_2O_3 in the fabrication of an electroluminescent device, where it was seen that at supercycle of $\text{Al}_2\text{O}_3:\text{Tb}_2\text{O}_3$ 4:2 was seen as the best alternative from several tested several supercycles, and the emission intensity was proven to be increasing with the injection current density.^[299] However, the lack of the long-wanted deep blue emitter has prevented achieving a full-color display.^[6]

7.2.2. MOSLEDs

MOSLEDs are attracting huge interest as light sources compatible with the CMOS (complementary metal oxide semiconductors) technology most relevant to applications such as telecommunication, waveguides, and micro-displays.^[144,186] Employment of ALD adds to the fabrication of MOSLEDs numerous benefits, including the ability to dope R^{3+} ions into several metal oxides. For example, Al_2O_3 has been considered as an attractive choice for the host material thanks to its wide transparency range and feasibility of ALD fabrication.^[147] In general, ALD offers a one-step fabrication technique for doped materials, for a wide range of host materials ranging from binary oxides to ternary oxides, and nanolaminates.^[33,307]

Among the most attractive dopants used in MOSLEDs are the NIR-emitting Yb^{3+} (emission at $\approx 980 \text{ nm}$) and Er^{3+} (emission at $\approx 1530 \text{ nm}$), the former used as a wave amplifier in lasers and the latter being essential for telecommunication applications as its emission lies in the NIR minimal loss window of silica-based optical fibers.^[334,335]

In Table 5, we summarize the MOSLED devices fabricated by ALD with Er^{3+} doping and their electrical performance. These

Table 5. Performance characteristics of Er^{3+} -based MOSLED devices fabricated by ALD: Annealing temperature of the films (Ann. T) external quantum efficiency (EQE), power efficiency (PE), threshold voltage (Vol), emission (1530–1550 nm) lifetime (τ), and operational device lifetime (OLT).

Matrix	Ann. T [°C]	EQE [%]	PE [$\times 10^{-4}$]	Vol [V]	τ [ms]	OLT [h]	Refs.
$\text{Y}_3\text{Ga}_5\text{O}_{12}$	800	2.5	3.8	25	2.26	49	[161]
$\text{Gd}_3\text{Ga}_5\text{O}_{12}$	1000	1.9	3.6	30	1.59	NG	[185]
ZnGa_2O_4	800	0.3	NG	30	0.82	5.5	[186]
$\text{Lu}_3\text{Al}_5\text{O}_{12}$	1100	10	12	50	1.65	NG	[150]
Yb_2O_3	1000	8.5	10	60	NG	NG	[148]
$\text{Yb}_3\text{Al}_5\text{O}_{12}$	1100	5.2	4.8	≈ 5	1.2	NG	[149]
Ga_2O_3	900	36	81	≈ 15	2.04	100	[145]
$\text{Al}_2\text{O}_3\text{-Y}_2\text{O}_3$	800	8.7	12	NG	NG	NG	[214]
$\text{Al}_2\text{O}_3\text{:Yb}$	NG	24	28	≈ 14	0.90	NG	[155]

MOSLEDS are typically evaluated based on their external quantum efficiency (EQE), which is also related to the power efficiency (PE) of the device, threshold voltage (Vol), the decay time of the Er^{3+} (1530–1550 nm) emission and the operational lifetime of the device. The threshold voltage is the minimum gate bias voltage required to achieve electroluminescence intensity, while the operational lifetime of the device is the duration through which the device maintains good stability (EL intensity at least equals 90% of the initial one) while working continuously.^[145]

7.2.3. White Light Emission

Light emitting materials are employed in a wide variety of applications that vary from light emitting diodes, displays, solar concentrator and biological imaging and photodynamic therapy.^[336] The sharp-line 4f–4f emissions of lanthanides and ultimately similar chemistry properties allow the combination of these emissions into a single phase tunable white light emission.^[337] White light generated from several different lanthanide components can be achieved through down-conversion or up-conversion, mixing ions that emit in red, green, and blue or alternatively yellow and blue. In down-conversion, Eu^{3+} is known for the red emission, while Tb^{3+} emits mainly in green and weaker emission in blue, and Dy^{3+} is a blue emitter.^[338,339] Blue emitters can also be combined with Sm^{3+} , which is known for its yellow–orange emission.^[340] On the other hand, in up-conversion, Er^{3+} is known to emit red and green with two-photon up-conversion and blue in three-photon up-conversion process. While Ho^{3+} also emits in red and green, Tm^{3+} emits in blue.^[140,341,342]

Luminescent displays fabricated by ALD have mainly depended on the electroluminescent materials of ZnS:Mn^{2+} and ZnS:Tb^{3+} that emit only in yellow and green, while a full color scale display is difficult to achieve due to the lack of deep blue emitters.^[6] Currently, the addition of red color from CaS:Eu^{3+} .^[64] However, very recently the white light emission could be demonstrated for ALD/MLD-grown (Tb, Eu, and Er)-TPA thin films, as seen in (Figure 13).^[316] The photoluminescence emission was shown to be somewhat tuneable, with emission properties comparable to commercial white light emissive LEDs, with a color rendering index of 88. This could open the door to using multi-

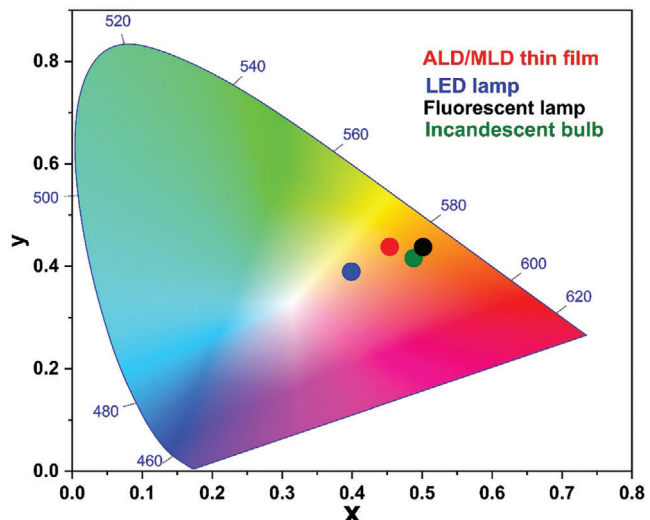


Figure 13. Emission color comparison: ALD/MLD grown (Tb,Eu,Er)-TPA thin film versus three different commercial white light emitting products: LED lamp, fluorescent lamp, and incandescent bulb.^[320]

lanthanide dopants in ALD and ALD/MLD to achieve white light emission.

7.2.4. Solar Cells

An intrinsic issue related to photovoltaics (PV) is that the current solar cell technologies mostly utilize the visible part of solar spectrum. To alleviate this issue, PV cells could be integrated with thin layers of IR-to-vis up-converting materials.^[18] Up-conversion is an anti-stokes process in which a photoactive ion absorbs two or more photons of low energy (in IR range) and then the absorbed energy is emitted as one photon of higher energy (in visible range). There are several more specific mechanisms described for the UC phenomenon that involve one or several types of Ln^{3+} ions.^[27,343] However, the most important design decision is the appropriate choice of the UC lanthanide species which depends on the type of the PV application targeted: Yb-based UC materials (IR abs. in 800–1000 nm) should be optimal for the wide-bandgap perovskite, dye-sensitized and organic PV devices, while in the case of the narrow-bandgap Si-based PVs, Yb-based up-converters do not add any benefit as silicon itself absorbs sun light up to 1100 nm (Figure 14).

The UC phenomenon has been realized for both ALD- and ALD/MLD-grown thin films based on Yb^{3+} as a sensitizer and Er^{3+} as an activator.^[147,321] These thin films could be beneficial to enhance the performance of dye-sensitized and perovskite solar cells, though this has not been demonstrated in practice so far. Most excitingly, ALD-grown Ho-doped Er_2O_3 thin films were recently successfully integrated with crystalline silicon solar cell (1.1 eV) technology, and an enhancement of $\approx 3\%$ in the short-circuit current density was demonstrated.^[140]

Besides the proper choice of the Ln species, another issue to be tackled is the characteristically low IR absorption capability of lanthanides in general. To overcome this, active research is going on, and organic molecules have been considered as sensitizers for the Ln upconverters.^[321] However, even though many

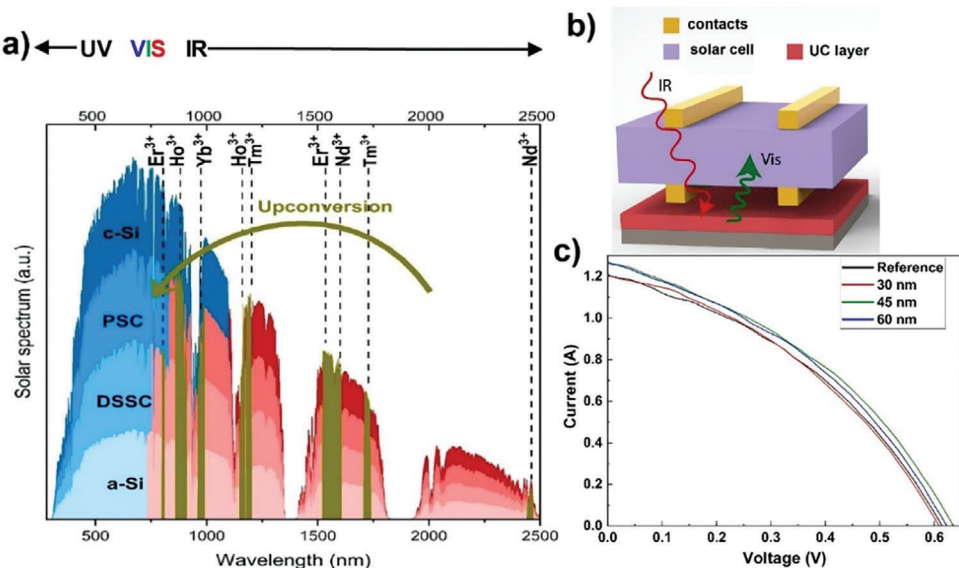


Figure 14. Scheme for UC-enhanced solar-cell performance: a) portions of the solar spectrum utilized by different solar cell technologies, and the potential to extend the usability with different UC Ln^{3+} ions, b) integration of UC layers into the solar cell device, and c) enhanced performance of c-Si solar cell achieved with ALD-grown UC $(\text{Er},\text{Ho})_2\text{O}_3$ coating with three different thicknesses. Reproduced with permission from Elsevier, 2021 refs.[18,140]

organics are strong IR absorbers, the conventional molecular Ln-organic complexes investigated have suffered from excitation energy losses due to the high-energy phonons. On the other hand, the first results for ALD/MLD-grown Ln-pyrazine thin films are highly promising as they showed intense IR-to-vis emission in the entire visible (blue-green-red) range.^[321] Tentatively, it is believed that in these hybrid thin films the organic ligands are bound more strongly to the Ln species such that the high-energy losses can be minimized.

In general, ALD is critical to next-generation solar cells, in particular all thin-film solar cells, additionally for current technologies the use of ALD-deposited Al_2O_3 for surface passivation,^[344] makes it more likely that ALD of R-based materials will continue their way toward better performing solar cells.

7.2.5. Biological Applications

Photoluminescent (UV-to-vis down-shifting) lanthanide ions have been widely investigated for various bio-imaging and bio-detection applications. However, the use of UV light damages most of the biological samples by photobleaching. Additionally, as biological samples may absorb the UV light, a so-called auto-fluorescence phenomenon may occur causing a large background noise that may be detrimental to the imaging.^[345] The use of UV is also limited to very low penetration depths, which makes e.g. deep tissue imaging immensely difficult.^[346]

To overcome the limitations related to the UV light excitation, novel lanthanide-based materials should be designed based on visible light (PL) or NIR (UC) excitation. Lanthanide-based UC materials may show enhanced depth penetration, thanks to the lower energy of NIR compared to UV.^[27] Also, the use of up-conversion in multimodal imaging can lead to better diagnostic tools as combining more than one imaging technique

that complements each other leads to better results.^[347] Hence the progress made in the ALD- and ALD/MLD-fabricated UC materials, i.e. $(\text{Yb},\text{Er})_2\text{O}_3$, $(\text{Er},\text{Ho})_2\text{O}_3$ and $(\text{Y},\text{Yb},\text{Er})\text{PZA}$ films, is of great promise,^[139,140,321] and the next step should be in testing them in biological imaging applications (Figure 15).

Down-conversion can also be used for the bio-detection of viruses and bio-assays of different ions, molecules, or tumor markers. Förster resonance energy transfer (FRET) is one of the strongly emerging techniques for bio-detection of viruses.^[348] In FRET, energy is transferred in a non-radiative way from one fluorophore (donor) to another fluorophore (acceptor) through dipole-coupling; the acceptor then emits this energy in a specified wavelength range.^[349] Lanthanide-organic hybrids are particularly promising as donor fluorophores in FRET.^[350] The distance between the donor and acceptor fluorophores in FRET plays a crucial role, as the efficiency of the transfer and subsequently, the emission is inversely proportional to the distance between the donor and acceptor; in other words, FRET can only be seen when this distance is less than 10 nm.^[351] Therefore, an ultrathin ALD/MLD-grown thin film could provide more stable emission and more efficient energy transfer in the FRET process compared to the present state-of-the-art efforts to utilize immobile (liquid-phase) donors. Very recently promising proof-of-concept data were obtained for Eu-HQA films grown from $\text{Eu}(\text{thd})_3$ and 2-hydroxyquinoline-4-carboxylic acid (HQA) precursors. In these thin films, the organic HQA component acts as a sensitizer for the red Eu^{3+} luminescence, extending the excitation wavelength range up to ca. 400 nm. Moreover, by depositing the films on nanoplasmonic structures emission intensity could be significantly (20-fold) enhanced. Finally, the FRET-type energy transfer process was demonstrated by combining the Eu-HQA coated nanoplasmonic structures with commercial Alexa647 fluorophor.^[55]

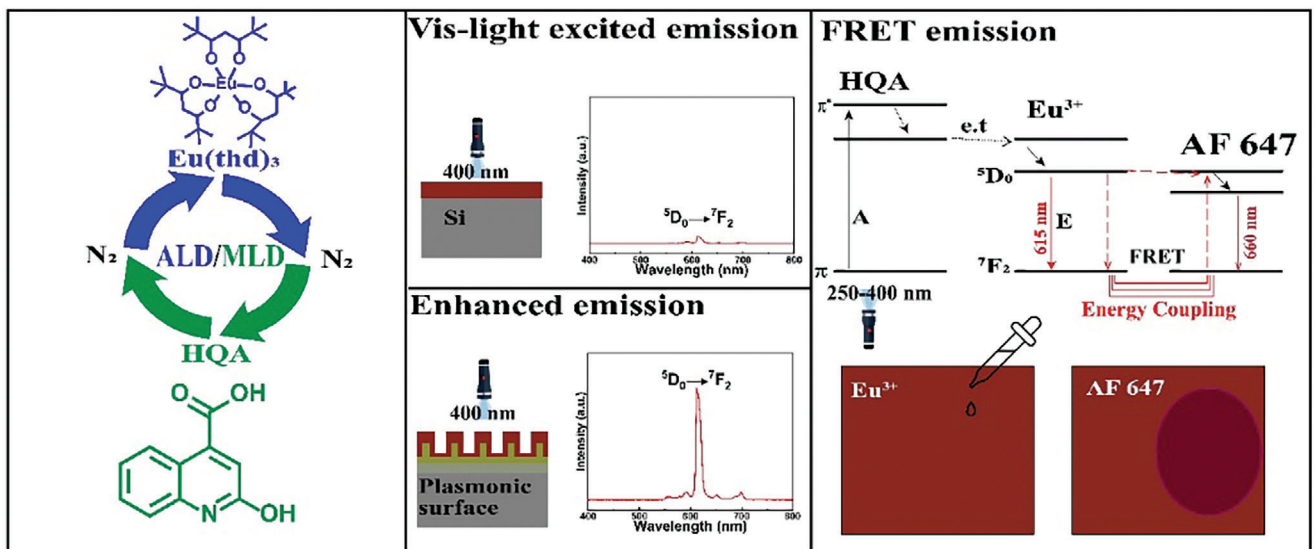


Figure 15. Scheme for FRET-based bio-detection of viruses: (left) ALD/MLD cycle for the growth of Eu-HQA thin films, (middle) enhancement of the red PL emission of Eu-HQA achieved by depositing the film on a nanoplasmonic substrate, and (right) principle of FRET mediated emission and its possible utilization bio-detection by using Eu-HQA as a donor chromophore and commercial AF 647 as an acceptor chromophore. (Reproduced under CC licence from ref. [55], 2023, Royal society of chemistry).

8. Conclusion and Outlook

A continuously broadening spectrum of ALD and later also MLD approaches for functional rare earth element-based thin films has been developed over the last three decades, fueled by various application expectations based on the many unique properties of these elements relevant to fields ranging from micro- and optoelectronics and solar energy conversion to medical diagnostics and different imaging and security technologies. Chemical composition-wise, rare earth elements have been employed both as dopants and main components in compounds ranging from metal oxides and fluorides to various metal-organic hybrids. In writing this review, our leading ambition was to provide the readers with a brief but at the same time comprehensive and insightful account of the overall progress in this scientifically significant and technologically prominent field.

Atomic layer deposition is known—owing to its capability to produce high-quality large-area homogeneous and conformal ultrathin films—as the state-of-the-art thin-film technology in microelectronics, but its unique benefits are also highly valued if not indispensable in many application areas involving the rare earth elements. From a historical perspective, in the first *R*-related ALD processes these elements were employed only as dopants in various electroluminescent thin films. Next, the interest gradually shifted to various ALD-grown R_2O_3 thin films investigated as a potential gate dielectric material replacement for SiO_2 in MOSFET transistor technology. This also led to fueling the research on rare earth precursors for better and faster ALD processes. Later, the major enthusiasm on this topic slowly faded away since even better-performing high-k dielectric materials were developed for which also more robust/beneficial ALD processes could be employed. In line with this progress, the interest in ALD of *R* oxide thin films expanded to more complex ternary and quaternary perovskite oxides with unique magnetic and catalytic properties.

More recently, researchers started to look for new solutions using the hardly matched optical properties of the lanthanide oxide thin films. To address this issue, new ALD processes were developed for lanthanide fluorides for various applications. Electroluminescence properties of Ln^{3+} ions in various matrices are of particular interest in applications such as telecommunications, screens, LEDs, and optical thermometry, thanks to their long luminescence lifetime and well-expected and controlled emission colors. This has led to a renewed interest in the use of Ln^{3+} ions as dopants in ALD thin films, particularly the use of Eu^{3+} for red light and Tb^{3+} for green light emissions. Moreover, Er^{3+} shows interesting emission characteristics near 1500 nm, relevant for the use in telecommunication and waveguide applications.

The most recent development highlighted in this review article is the rapidly expanding family of novel ALD/MLD-grown lanthanide-organic thin-film materials with exciting luminescence properties. Thanks to their remarkable photoluminescence and up-conversion characteristics that seem to be hard to meet with purely inorganic thin films, lanthanide-organic thin films are anticipated to provide new horizons for e.g. lighting, imaging, and solar cell applications. These hybrid thin films also possess significantly enhanced mechanical properties added by the organic component. Thus, they are interesting candidates for next-generation flexible devices, such as all-thin-film solar cells. Additionally, depending on the choice of the organic component, it may act as an efficient sensitizer for the Ln^{3+} luminescence in the Ln-organic hybrid coating, such that the excitation wavelength range can be extended from the UV light to visible light. To bring these novel material candidates closer to their true applications there are however several practical issues to be tackled, such as their long-term stability. On the other hand, an interesting aspect little emphasized so far is the fact that the ALD/MLD processes are fundamentally more economical than the ALD processes, as

the film growth rates are considerably higher in ALD/MLD and the deposition temperatures considerably lower, allowing shorter processing times (needed to reach the target film thickness); this can save time and energy, reduce the consumption of relatively expensive rare earth precursors, and offer a path to reduce the environmental impact.^[352]

In general, the possibility to use lower deposition temperatures is beneficial for the larger-scale processing, not only from the energy saving point of view but also because it allows the use of temperature-sensitive substrates. Yet, the low vapor pressures typical for many organic precursors may pose some limitations in the precursor selection on a large scale and the challenge to find precursors with matching chemical reactivity toward co-reactants of interest for established and novel material systems persists nowadays, as much as it existed in the earlier days of precursor and process development for rare earth materials. Especially for hybrid ALD/MLD thin films in which an organic co-reactant plays a tremendous role, some inspiration for future precursor and process design could be drawn by reconsidering chemical fundamentals in the form of the simple acid–base concept according to Brønsted.^[353] Interestingly, the successful employment of the $R(\text{amd})(\text{Cp})_2$ precursor class, often perceived as the most balanced one for the ALD of inorganic R -based materials, has yet to be demonstrated. As illustrated in this review, hybrid thin film growth has rather been realized with $R(\text{thd})_x$ and $R(\text{guan})_3$ precursors, whereby the latter facilitated significantly higher GPCs in the few cases they were tested already. It seems thus plausible that all-nitrogen containing R precursor classes such as the guanidinates or formamidinates may experience more utilization in future proof-of-concept studies. In summary, much remains to be done for academia and industry alike to enable true breakthroughs for ALD/MLD rare earth element containing thin films in emerging applications. First, by far more processes employing especially the nitrogen and all-nitrogen containing R precursor classes need to be developed and benchmarked against the already reported hybrid processes. Secondly, research and development efforts need to be brought to the next processing level meaning that academic reports on the matter need to trigger industrial concept and feasibility studies on industrially relevant ALD/MLD deposition equipment. Only then productization will become viable.

Supporting Information

Supporting Information is available from the Wiley Online Library or from the author.

Acknowledgements

Funding was received from the European Union (ERC AdG, UniEnMLD, No. 101097815). Views and opinions expressed are however those of the authors only and do not necessarily reflect those of the European Union or the European Research Council. Neither the European Union nor the granting authority can be held responsible for them. A.D. thanks the Leibniz Association, Attract Funding of Fraunhofer and Ruhr University Bochum (RUB) for supporting this work. A. D. and M. K. are grateful to the DAAD and Academy of Finland for funding the ALPMOH project (57610451).

Open access funding enabled and organized by Projekt DEAL.

Conflict of Interest

The authors declare no conflict of interest.

Keywords

atomic layer deposition, lanthanides, molecular layer deposition, rare earth elements, thin films

Received: March 29, 2024

Revised: July 5, 2024

Published online: August 23, 2024

- [1] T. Suntola, *Sci Rep* **1989**, *4*, 261.
- [2] H. H. Sønsteby, A. Yanguas-Gil, J. W. Elam, *J Vac Sci Technol A* **2020**, *38*, 020804.
- [3] N. E. Richey, C. De Paula, S. F. Bent, *J. Chem. Phys.* **2020**, *152*, 040902.
- [4] Y. Zhao, L. Zhang, J. Liu, K. Adair, F. Zhao, Y. Sun, T. Wu, X. Bi, K. Amine, J. Lu, X. Sun, *Chem. Soc. Rev.* **2021**, *50*, 3889.
- [5] T. S. Tripathi, M. Karppinen, *Adv. Mater. Interfaces* **2017**, *4*, 1700300.
- [6] M. Leskelä, M. Mattinen, M. Ritala, *J. Vac. Sci. Technol. B* **2019**, *37*, 030801.
- [7] V. Zardetto, B. L. Williams, A. Perrotta, F. Di Giacomo, M. A. Verheijen, R. Andriessen, W. M. M. Kessels, M. Creatore, *Sustain. Energy Fuels* **2017**, *1*, 30.
- [8] S. Seo, S. Jeong, H. Park, H. Shin, N. G. Park, *Chem. Commun.* **2019**, *55*, 2403.
- [9] J. A. Raiford, S. T. Oyakhire, S. F. Bent, *Energy Environ. Sci.* **2020**, *13*, 1997.
- [10] T. Jussila, A. Philip, T. Tripathi, K. Nielsch, M. Karppinen, *Appl. Phys. Rev.* **2023**, *10*, 41313.
- [11] J. P. Niemelä, A. J. Karttunen, M. Karppinen, *J. Mater. Chem. C* **2015**, *3*, 10349.
- [12] M. Madadi, J. Heiska, J. Multia, M. Karppinen, *ACS Appl. Mater. Interfaces* **2021**, *13*, 56793.
- [13] D. J. Hagen, M. E. Pemble, M. Karppinen, *Appl. Phys. Rev.* **2019**, *6*, 041309.
- [14] T. Tytell, M. Karppinen, *Semicond. Sci. Technol.* **2014**, *29*, 043001.
- [15] J. P. Niemelä, G. Marin, M. Karppinen, *Semicond. Sci. Technol.* **2017**, *32*, 093005.
- [16] G. Dingemans, W. M. M. Kessels, *J Vac Sci Technol A* **2012**, *30*, 040802.
- [17] J. C. G. Bünzli, *Coord. Chem. Rev.* **2015**, *19*, 293.
- [18] A. Ghazy, M. Safdar, M. Lastusaari, H. Savin, M. Karppinen, *Sol. Energy Mater. Sol. Cells* **2021**, *230*, 111234.
- [19] J. C. G. Bünzli, S. V. Eliseeva, *Chem. Sci.* **2013**, *4*, 1939.
- [20] T. Behrsing, G. B. Deacon, P. C. Junk, in *R-E-B C. Inhib.*, (Eds.: M. Forsyth, B. Hinton), Woodhead Publishing, Cambridge, UK **2014**, pp. 1–37.
- [21] S. V. Eliseeva, *Luminescence of Lanthanide Ions in Coordination Compounds and Nanomaterials* (Ed.: A. Bettencourt-Dias), Wiley, Hoboken, New Jersey **2015**.
- [22] Y. Charreire, A. Marbeuf, G. Tourillon, M. Leskelä, L. Niinistö, E. Nykänen, P. Soininen, O. Tolonen, *J. Electrochem. Soc.* **1992**, *139*, 619.
- [23] Y. Charreire, O. Tolonen-Kivimäki, E. Nykänen, M. Leskelä, L. Niinistö, D. Bonnin, O. Heckmann, *Thin Solid Films* **1994**, *247*, 151.
- [24] S. M. George, B. H. Lee, B. Yoon, A. I. Abdulagatov, R. A. Hall, *J. Nanosci. Nanotechnol.* **2011**, *11*, 7948.
- [25] T. Tytell, M. Karppinen, in *Oxide Thin Films Multilayers Nanocomposites*, Springer International Publishing, Cham **2015**, pp. 157–179.

- [26] K. Gregorczyk, M. Knez, *Prog. Mater. Sci.* **2016**, *75*, 1.
- [27] M. Safdar, A. Ghazy, M. Lastusaari, M. Karppinen, *J. Mater. Chem. C* **2020**, *8*, 6946.
- [28] M. Nieminen, M. Putkonen, L. Niinistö, *Appl. Surf. Sci.* **2001**, *174*, 155.
- [29] R. L. Puurunen, A. Delabie, S. Van Elshocht, M. Caymax, M. L. Green, B. Brijs, O. Richard, H. Bender, T. Conard, I. Hoflijk, W. Vandervorst, D. Hellin, D. Vanhaeren, C. Zhao, S. De Gendt, M. Heyns, *Appl. Phys. Lett.* **2005**, *86*, 073116.
- [30] S. M. George, *Chem. Rev.* **2010**, *110*, 111.
- [31] M. Leskelä, M. Ritala, *Thin Solid Films* **2002**, *409*, 138.
- [32] E. Ahvenniemi, M. Matvejeff, M. Karppinen, *Dalton Trans.* **2015**, *44*, 8001.
- [33] H. Wang, J. J. Wang, R. Gordon, J. S. M. Lehn, H. Li, D. Hong, D. V. Shenai, *Electrochim. Solid-State Lett.* **2009**, *12*, G13.
- [34] A. Tammi, M. Heikkilä, M. Kernell, J. Kozlova, K. Kukli, V. Sammelselg, M. Ritala, M. Leskelä, *Thin Solid Films* **2010**, *519*, 666.
- [35] T. Yoshiimura, S. Tatsuura, W. Sotoyama, *Appl. Phys. Lett.* **1991**, *59*, 482.
- [36] P. Sundberg, M. Karppinen, *Beilstein J. Nanotechnol.* **2014**, *5*, 1104.
- [37] J. Multia, M. Karppinen, *Adv. Mater. Interfaces* **2022**, *9*, 2200210.
- [38] A. Khayyami, A. Philip, M. Karppinen, *Angew. Chem. – Int. Ed.* **2019**, *58*, 13400.
- [39] A. Philip, J. P. Niemelä, G. C. Tewari, B. Putz, T. E. J. Edwards, M. Itoh, I. Utke, M. Karppinen, *ACS Appl. Mater. Interfaces* **2020**, *12*, 21912.
- [40] B. H. Lee, B. Yoon, V. R. Anderson, S. M. George, *J. Phys. Chem. C* **2012**, *116*, 3250.
- [41] A. J. Karttunen, L. Sarnes, R. Townsend, J. Mikkonen, M. Karppinen, *Adv. Electron. Mater.* **2017**, *3*, 1600459.
- [42] R. M. Silva, J. Rocha, R. F. Silva, *Nanoscale* **2023**, *15*, 10423.
- [43] Z. Giedraityte, P. Sundberg, M. Karppinen, *J. Mater. Chem. C* **2015**, *3*, 12316.
- [44] A. Philip, R. Ghiyasi, M. Karppinen, *Molecules* **2021**, *26*, 3214.
- [45] L. Momtazi, H. H. Sønsteby, O. Nilsen, *Beilstein J. Nanotechnol.* **2019**, *9*, 399.
- [46] L. Momtazi, D. A. Dartt, O. Nilsen, J. R. Eidet, *J. Biomed. Mater. Res. – Part A* **2018**, *106*, 3090.
- [47] Z. Giedraityte, J. Sainio, D. Hagen, M. Karppinen, *J. Phys. Chem. C* **2017**, *121*, 17538.
- [48] Z. Giedraityte, O. Lopez-Acevedo, L. A. Espinosa Leal, V. Pale, J. Sainio, T. S. Tripathi, M. Karppinen, *J. Phys. Chem. C* **2016**, *120*, 26342.
- [49] E. Ahvenniemi, M. Karppinen, *Chem. Mater.* **2016**, *28*, 6260.
- [50] R. L. Puurunen, *Chem. Vap. Depos.* **2003**, *9*, 327.
- [51] R. W. Johnson, A. Hultqvist, S. F. Bent, *Mater. Today* **2014**, *17*, 236.
- [52] A. C. Jones, H. C. Aspinall, P. R. Chalker, R. J. Potter, K. Kukli, A. Rahtu, M. Ritala, M. Leskelä, *Mater Sci Eng B Solid State Mater Adv Technol* **2005**, *118*, 97.
- [53] N. Boysen, D. Zanders, T. Berning, S. M. J. Beer, D. Rogalla, C. Bock, A. Devi, *RSC Adv.* **2021**, *11*, 2565.
- [54] L. Mai, N. Boysen, E. Subaşı, T. De Los Arcos, D. Rogalla, G. Grundmeier, C. Bock, H. L. Lu, A. Devi, *RSC Adv.* **2018**, *8*, 4987.
- [55] A. Ghazy, J. Ylönen, N. Subramaniyan, M. Karppinen, *Nanoscale* **2023**, *15*, 15865.
- [56] T. Hatanpää, M. Ritala, M. Leskelä, *Coord. Chem. Rev.* **2013**, *257*, 3297.
- [57] A. Devi, *Coord. Chem. Rev.* **2013**, *257*, 3332.
- [58] H. Mölsä, L. Niinistö, M. Utrainen, *Adv Mater* **1994**, *4*, 389.
- [59] S. Haukka, T. Suntola, *Interface Sci.* **1997**, *5*, 119.
- [60] H. Seim, H. Mölsä, M. Nieminen, H. Fjellvåg, L. Niinistö, *J. Mater. Chem.* **1997**, *7*, 449.
- [61] P. Kaur, A. Muriqi, J. L. Wree, R. Ghiyasi, M. Safdar, M. Nolan, M. Karppinen, A. Devi, *Dalton Trans.* **2022**, *51*, 5603.
- [62] Z. Fang, P. A. Williams, R. Odedra, H. Jeon, R. J. Potter, *J. Cryst. Growth* **2012**, *338*, 111.
- [63] E. Atosuo, K. Mizohata, M. Mattinen, M. Mäntymäki, M. Vehkämäki, M. Leskelä, M. Ritala, *J. Vac. Sci. Technol. A* **2022**, *40*, 022402.
- [64] J. Rosa, J. Lahtinen, J. Julin, Z. Sun, H. Lipsanen, *Materials* **2021**, *14*, 5966.
- [65] J. Robertson, *Rep. Prog. Phys.* **2005**, *69*, 327.
- [66] G. D. Wilk, R. M. Wallace, J. M. Anthony, *J. Appl. Phys.* **2001**, *89*, 5243.
- [67] M. Leskelä, M. Ritala, *J. Solid State Chem.* **2003**, *171*, 170.
- [68] S. Ohmi, C. Kobayashi, I. Kashiwagi, C. Ohshima, H. Ishiwara, H. Iwai, *J. Electrochem. Soc.* **2003**, *150*, F134.
- [69] J. Shi, Y. Hou, W. Chu, X. Shi, H. Gu, B. Wang, Z. Sun, *Inorg. Chem.* **2013**, *52*, 5013.
- [70] K. Nehra, A. Dalal, A. Hooda, S. Bhagwan, R. K. Saini, B. Mari, S. Kumar, D. Singh, *J. Mol. Struct.* **2022**, *1249*, 131531.
- [71] T. Phillips, D. E. Sands, W. F. Wagner, *Inorg. Chem.* **1968**, *7*, 2295.
- [72] B. A. J. Cunningham, D. E. Sands, *Inorg. Chem.* **1967**, *6*, 499.
- [73] G. A. M. Hussein, H. M. Ismail, *Powder Technol.* **1995**, *84*, 185.
- [74] D. Barreca, G. A. Battiston, D. Berto, R. Gerbasi, E. Tondello, *Surf. Sci. Spectra* **2001**, *8*, 234.
- [75] G. Malandrino, R. Lo Nigro, C. Benelli, F. Castelli, I. L. Fragalà, *Chem. Vap. Depos.* **2000**, *6*, 233.
- [76] C. Elschenbroich, *Organometallics*, 3rd ed., Wiley, Hoboken, NJ **2006**.
- [77] T. Cuenca, P. Royo, *Coord. Chem. Rev.* **1999**, *193–195*, 447.
- [78] T. Blanquart, M. Kaipio, J. Niinistö, M. Gavagnin, V. Longo, L. Blanquart, C. Lansalot, W. Noh, H. D. Wanzenböck, M. Ritala, M. Leskelä, *Chem. Vap. Depos.* **2014**, *20*, 217.
- [79] S. Dueñas, H. Castán, H. García, A. Gómez, L. Bailón, K. Kukli, J. Aarik, M. Ritala, M. Leskelä, *J. Electrochem. Soc.* **2008**, *155*, G241.
- [80] H. L. Lu, G. Scarel, L. Lamagna, M. Fanciulli, S. J. Ding, D. W. Zhang, *Appl. Phys. Lett.* **2008**, *93*, 152906.
- [81] G. Scarel, C. Wiemer, M. Fanciulli, I. L. Fedushkin, G. K. Fukin, G. A. Domrachev, Y. Lebedinskii, A. Zenkevich, G. Pavia, Z. Anorg. Allg. Chem. **2007**, *633*, 2097.
- [82] J. Päiväsari, M. Putkonen, L. Niinistö, *Thin Solid Films* **2005**, *472*, 275.
- [83] J. Niinistö, N. Petrova, M. Putkonen, L. Niinistö, K. Arstila, T. Sajavaara, *J. Cryst. Growth* **2005**, *285*, 191.
- [84] J. Päiväsari, M. Putkonen, T. Sajavaara, L. Niinistö, *J. Alloys Compd.* **2004**, *374*, 124.
- [85] J. S. Wrench, K. Black, H. C. Aspinall, A. C. Jones, J. Bacsa, P. R. Chalker, P. J. King, M. Werner, H. O. Davies, P. N. Heys, *Chem. Vap. Depos.* **2009**, *15*, 259.
- [86] J. Päiväsari, J. Niinistö, K. Arstila, K. Kukli, M. Putkonen, L. Niinistö, *Chem. Vap. Depos.* **2005**, *11*, 415.
- [87] R. Xu, Q. Tao, Y. Yang, C. G. Takoudis, *Appl. Surf. Sci.* **2012**, *258*, 8514.
- [88] B. Kaczer, J. Franco, P. Weckx, P. J. Roussel, V. Putcha, E. Bury, M. Simicic, A. Chasin, D. Linten, B. Parvais, F. Catthoor, G. Rzepa, M. Waltl, T. Grasser, *Microelectron Reliab.* **2018**, *81*, 186.
- [89] M. Houssa, G. Pourtois, M. M. Heyns, A. Stesmans, *J. Phys. Condens. Matter* **2005**, *17*, S2075.
- [90] A. F. Holleman, E. Wiberg, N. Wiberg, *Lehrb. Anorg. Chem.* **2007**, *102*, 1315.
- [91] M. Lappert, A. Protchenko, P. P. Power, A. Seeber, *Metal Amide Chemistry*, Wiley, Hoboken, NJ **2009**.
- [92] D. Zanders, G. Bačić, D. Leckie, O. Odegbesan, J. Rawson, J. D. Masuda, A. Devi, S. T. Barry, *Angew. Chem., Int. Ed.* **2020**, *59*, 14138.
- [93] M. Brookhart, M. L. H. Green, G. Parkin, *Proc. Natl. Acad. Sci. USA* **2007**, *104*, 6908.
- [94] K. Kukli, M. Ritala, T. Pilvi, T. Sajavaara, M. Leskelä, A. C. Jones, H. C. Aspinall, D. C. Gilmer, P. J. Tobin, *Chem. Mater.* **2004**, *16*, 5162.

- [95] D. H. Triyoso, R. I. Hegde, J. M. Grant, J. K. Schaeffer, D. Roan, B. E. White, P. J. Tobin, *J Vac Sci Technol B Microelectron Nanometer Struct Process Meas Phenom* **2005**, *23*, 288.
- [96] R. J. Potter, P. R. Chalker, T. D. Manning, H. C. Aspinall, Y. F. Loo, A. C. Jones, L. M. Smith, G. W. Critchlow, M. Schumacher, *Chem. Vap. Depos.* **2005**, *11*, 159.
- [97] K. Kukli, T. Hatanpää, M. Ritala, M. Leskelä, *Chem. Vap. Depos.* **2007**, *13*, 546.
- [98] B. S. Lim, A. Rahtu, R. G. Gordon, *Nat. Mater.* **2003**, *2*, 749.
- [99] B. S. Lim, A. Rahtu, J. S. Park, R. G. Gordon, *Inorg. Chem.* **2003**, *42*, 7951.
- [100] P. De Rouffignac, J. S. Park, R. G. Gordon, *Chem. Mater.* **2005**, *17*, 4808.
- [101] J. Päiväsäari, C. L. Dezelah IV, D. Back, H. M. El-Kaderi, M. J. Heeg, M. Putkonen, L. Niinistö, C. H. Winter, *J. Mater. Chem.* **2005**, *15*, 4224.
- [102] P. De Rouffignac, R. G. Gordon, *Chem. Vap. Depos.* **2006**, *12*, 152.
- [103] K. H. Kim, D. B. Farmer, J. S. M. Lehn, P. Venkateswara Rao, R. G. Gordon, *Appl. Phys. Lett.* **2006**, *89*, 133512.
- [104] P. De Rouffignac, A. P. Yousef, K. H. Kim, R. G. Gordon, *Electrochem. Solid-State Lett.* **2006**, *9*, F45.
- [105] L. Du, K. Wang, Y. Zhong, B. Liu, X. Liu, Y. Ding, *J. Mater. Sci.* **2020**, *55*, 5378.
- [106] S. B. Kim, A. Jayaraman, D. Chua, L. M. Davis, S. L. Zheng, X. Zhao, S. Lee, R. G. Gordon, *Chemistry* **2018**, *24*, 9525.
- [107] K. Xu, R. Ranjith, A. Laha, H. Parala, A. P. Milanov, R. A. Fischer, E. Bugiel, J. Feydt, S. Irsen, T. Toader, C. Bock, D. Rogalla, H. J. Osten, U. Kunze, A. Devi, *Chem. Mater.* **2012**, *24*, 651.
- [108] K. Xu, A. R. Chaudhuri, H. Parala, D. Schwendt, T. D. L. Arcos, H. J. Osten, A. Devi, *J. Mater. Chem. C* **2013**, *1*, 3939.
- [109] A. P. Milanov, K. Xu, A. Laha, E. Bugiel, R. Ranjith, D. Schwendt, H. J. Osten, H. Parala, R. A. Fischer, A. Devi, *J. Am. Chem. Soc.* **2010**, *132*, 36.
- [110] L. Mai, Z. Giedraityte, M. Schmidt, D. Rogalla, S. Scholz, A. D. Wieck, A. Devi, M. Karppinen, *J. Mater. Sci.* **2017**, *52*, 6216.
- [111] A. Kurek, P. G. Gordon, S. Karle, A. Devi, S. T. Barry, *Aust. J. Chem.* **2014**, *67*, 989.
- [112] S. E. Koponen, P. G. Gordon, S. T. Barry, *Polyhedron* **2016**, *108*, 59.
- [113] B. Lee, T. J. Park, A. Hande, M. J. Kim, R. M. Wallace, J. Kim, X. Liu, J. H. Yi, H. Li, M. Rousseau, D. Shenai, J. Suydam, *Microelectron. Eng.* **2009**, *86*, 1658.
- [114] S. M. J. Beer, N. Boysen, A. Muriqi, D. Zanders, T. Berning, D. Rogalla, C. Bock, M. Nolan, A. Devi, *Dalton Trans.* **2021**, *50*, 12944.
- [115] M. Golalikhani, T. James, P. Van Buskirk, W. Noh, J. Lee, Z. Wang, J. F. Roeder, *J Vac Sci Technol A* **2018**, *36*, 051502.
- [116] S. Seppälä, J. Niinistö, M. Mattinen, K. Mizohata, J. Räisänen, W. Noh, M. Ritala, M. Leskelä, *Thin Solid Films* **2018**, *660*, 199.
- [117] J. S. Lee, W. H. Kim, I. K. Oh, M. K. Kim, G. Lee, C. W. Lee, J. Park, C. Lansalot-Matras, W. Noh, H. Kim, *Appl. Surf. Sci.* **2014**, *297*, 16.
- [118] S. Seppälä, J. Niinistö, T. Blanquart, M. Kaipio, K. Mizohata, J. Räisänen, C. Lansalot-Matras, W. Noh, M. Ritala, M. Leskelä, *Chem. Mater.* **2016**, *28*, 5440.
- [119] I. S. Park, Y. C. Jung, S. Seong, J. Ahn, J. Kang, W. Noh, C. Lansalot-Matras, *J. Mater. Chem. C* **2014**, *2*, 9240.
- [120] B. Zhao, F. Mattelaer, G. Rampelberg, J. Dendooven, C. Detavernier, *ACS Appl. Mater. Interfaces* **2020**, *12*, 3179.
- [121] S. T. Barry, *Chemistry of Atomic Layer Deposition*, De Gruyter, Berlin, Germany **2022**.
- [122] K. Bernal Ramos, M. J. Saly, Y. J. Chabal, *Coord. Chem. Rev.* **2013**, *257*, 3271.
- [123] G. K. Mussabek, D. Yermukhamed, K. K. Dikhanbayev, al. . , J. Key Lee, M.-S. Lee, S. Hong, J. Li, G. Chai, X. Wang, G. V. Kunte, S. A. Shivashankar, A. M. Umarji, *Meas. Sci. Technol.* **2008**, *19*, 025704.
- [124] P. Kaur, L. Mai, A. Muriqi, D. Zanders, R. Ghiyasi, M. Safdar, N. Boysen, M. Winter, M. Nolan, M. Karppinen, A. Devi, *Chemistry* **2021**, *27*, 4913.
- [125] M. Putkonen, M. Nieminen, J. Niinistö, L. Niinistö, T. Sajavaara, *Chem. Mater.* **2001**, *13*, 4701.
- [126] A. Kosola, J. Päiväsäari, M. Putkonen, L. Niinistö, *Thin Solid Films* **2005**, *479*, 152.
- [127] N. A. Stafford, R. Katamreddy, L. Guerin, B. Feist, C. Dussarrat, *ECS Meet. Abstr.* **2009**, MA2009-01, 821.
- [128] R. Xu, S. K. Selvaraj, N. Azimi, C. G. Takoudis, *ECS Meet. Abstr.* **2012**, MA2012-02, 2467.
- [129] J. Kwon, M. Dai, M. D. Halls, E. Langereis, Y. J. Chabal, R. G. Gordon, *J. Phys. Chem. C* **2009**, *113*, 654.
- [130] K. Kukli, H. Heikkilä, E. Nykänen, L. Niinistö, *J. Alloys Compd.* **1998**, *275*–277, 10.
- [131] K. Kukli, M. Peussa, L. S. Johansson, E. Nykänen, L. Niinistö, *Mater. Sci. Forum* **1999**, *315*–317, 216.
- [132] T. Pilvi, E. Puukilainen, F. Munnik, M. Leskelä, M. Ritala, *Chem. Vap. Depos.* **2009**, *15*, 27.
- [133] T. Pilvi, E. Puukilainen, K. Arstila, M. Leskelä, M. Ritala, *Chem. Vap. Depos.* **2008**, *14*, 85.
- [134] E. Atosuo, M. Mäntymäki, L. Pesonen, K. Mizohata, T. Hatanpää, M. Leskelä, M. Ritala, *Dalton Trans.* **2023**, *52*, 10844.
- [135] L. Nyns, X. Shi, H. Tiemens, S. Van Elshocht, L. Date, R. Schreutelkamp, *J. Vac. Sci. Technol. Vac. Surf. Films* **2012**, *30*, 01A120.
- [136] E. Balée, A. Ringuedé, M. Cassir, M. Putkonen, L. Niinistö, *Chem. Mater.* **2009**, *21*, 4614.
- [137] A. Tamm, J. Kozlova, T. Arroval, L. Aarik, P. Ritslaid, H. García, H. Castán, S. Dueñas, K. Kukli, J. Aarik, *Chem. Vap. Depos.* **2015**, *21*, 181.
- [138] J. M. Gaskell, A. C. Jones, H. C. Aspinall, S. Przybylak, P. R. Chalker, K. Black, H. O. Davies, P. Taechakumput, S. Taylor, G. W. Critchlow, *J. Mater. Chem.* **2006**, *16*, 3854.
- [139] M. Tuomisto, Z. Giedraityte, M. Karppinen, M. Lastusaari, *Phys Status Solidi Rapid Res Lett* **2017**, *11*, 1700076.
- [140] A. Ghazy, M. Safdar, M. Lastusaari, A. Aho, A. Tukiainen, H. Savin, M. Guina, M. Karppinen, *Sol. Energy Mater. Sol. Cells* **2021**, *219*, 110787.
- [141] M. N. Getz, P. A. Hansen, Ø. S. Fjellvåg, M. A. K. Ahmed, H. Fjellvåg, O. Nilsen, *J. Mater. Chem. C* **2017**, *5*, 8572.
- [142] M. N. Getz, O. Nilsen, P.-A. Hansen, *Sci. Rep.* **2019**, *9*, 10247.
- [143] M. Y. Arsent'ev, M. V. Kalinina, P. A. Tikhonov, L. V. Morozova, T. L. Egorova, O. A. Shilova, *Glass Phys. Chem.* **2014**, *40*, 629.
- [144] K. Solehmainen, M. Kapulainen, P. Heimala, K. Polamo, *IEEE Photonics Technol. Lett.* **2004**, *16*, 194.
- [145] L. Yang, J. Xu, K. Yuan, Y. Yang, J. Sun, *Appl. Phys. Lett.* **2021**, *118*, 141104.
- [146] J. Rosa, M. J. Heikkilä, M. Sirkia, S. Merdes, *Materials* **2021**, *14*, 1505.
- [147] Z. Ouyang, Y. Yang, J. Sun, *Scr. Mater.* **2018**, *151*, 1.
- [148] Z. Ouyang, Y. Yang, J. Sun, *Opt. Mater.* **2018**, *80*, 209.
- [149] J. Liu, Z. Ouyang, Y. Yang, J. Sun, *J. Alloys Compd.* **2020**, *832*, 154964.
- [150] J. Xu, L. Yang, Z. Ma, Y. Yang, J. Sun, *J. Alloys Compd.* **2021**, *885*, 160993.
- [151] T. P. Holme, C. Lee, F. B. Prinz, *Solid State Ion.* **2008**, *179*, 1540.
- [152] C. C. Chao, Y. B. Kim, F. B. Prinz, *Nano Lett.* **2009**, *9*, 3626.
- [153] C. N. Ginestra, R. Sreenivasan, A. Karthikeyan, S. Ramanathan, P. C. McIntyre, *Electrochem. Solid-State Lett.* **2007**, *10*, B161.
- [154] Y. Charreire, R. Cortes, E. Nykänen, L. Niinistö, P. Soininen, M. Leskelä, *Fresenius J Anal Chem* **1998**, *362*, 41.
- [155] Y. Yang, Z. Ouyang, J. Liu, J. Sun, *Phys Status Solidi Rapid Res Lett* **2019**, *13*, 1900137.
- [156] N. Al Helou, L. Khomenkova, E. Cadel, C. Labbé, J. Cardin, F. Gourbilleau, E. Talbot, *Mater. Sci. Eng. B* **2023**, *296*, 116672.
- [157] T. T. Van, J. P. Chang, *Appl. Phys. Lett.* **2005**, *87*, 011907.

- [158] T. T. Van, J. R. Bargar, J. P. Chang, *J. Appl. Phys.* **2006**, *100*, 023115.
- [159] T. T. Van, J. Hoang, R. Ostroumov, K. L. Wang, J. R. Bargar, J. Lu, H. O. Blom, J. P. Chang, *J. Appl. Phys.* **2006**, *100*, 073512.
- [160] J. Hoang, T. T. Van, M. Sawkar-Mathur, B. Hoex, M. C. M. Van De Sanden, W. M. M. Kessels, R. Ostroumov, K. L. Wang, J. R. Bargar, J. P. Chang, *J. Appl. Phys.* **2007**, *101*, 123116.
- [161] Z. Yu, K. Yuan, Y. Yang, J. Sun, *Nanoscale* **2022**, *14*, 10540.
- [162] L. Lamagna, C. Wiemer, S. Baldovino, A. Molle, M. Perego, S. Schamm-Chardon, P. E. Coulon, M. Fanciulli, *Appl. Phys. Lett.* **2009**, *95*, 122902.
- [163] J. H. Shim, J. S. Park, J. An, T. M. Gür, S. Kang, F. B. Prinz, *Chem. Mater.* **2009**, *21*, 3290.
- [164] J. Niinistö, K. Kukli, T. Sajavaara, M. Ritala, M. Leskelä, L. Oberbeck, J. Sundqvist, U. Schröder, *Electrochem. Solid-State Lett.* **2008**, *12*, G1.
- [165] Q. Tao, G. Jursich, P. Majumder, M. Singh, W. Walkusz, P. Gu, R. Klie, C. Takoudis, *Electrochem. Solid-State Lett.* **2009**, *12*, G50.
- [166] P. Majumder, G. Jursich, C. Takoudis, *J. Appl. Phys.* **2009**, *105*, 104106.
- [167] J. Gluch, T. Rößler, S. B. Menzel, J. Eckert, *Microelectron. Eng.* **2011**, *88*, 561.
- [168] L. Wu, H. Y. Yu, K. L. Pey, J. S. Pan, M. Tuominen, E. Tois, D. Y. Lee, K. Y. Hsu, K. T. Huang, H. J. Tao, Y. J. Mii, *Electrochem. Solid-State Lett.* **2010**, *13*, G21.
- [169] C. Wiemer, L. Lamagna, S. Baldovino, M. Perego, S. Schamm-Chardon, P. E. Coulon, O. Salicio, G. Congedo, S. Spiga, M. Fanciulli, *Appl. Phys. Lett.* **2010**, *96*, 182901.
- [170] C. Adelmann, H. Tiemens, D. Dewulf, A. Hardy, D. Pierreux, J. Swerts, E. Rosseel, X. Shi, M. K. Van Bael, J. A. Kittl, S. Van Elshocht, *J. Electrochem. Soc.* **2010**, *157*, G105.
- [171] T. Wang, J. G. Ekerdt, *Chem. Mater.* **2009**, *21*, 3096.
- [172] T. Wang, J. G. Ekerdt, *Chem. Mater.* **2010**, *22*, 3798.
- [173] L. Aarik, K. Peetermann, L. Puust, H. Mändar, A. Kikas, I. Sildos, J. Aarik, *J. Alloys Compd.* **2021**, *868*, 159100.
- [174] K. Kukli, L. Aarik, G. Vinuesa, S. Dueñas, H. Castán, H. García, A. Kasikov, P. Ritslaid, H. M. Piirsoo, J. Aarik, *Materials* **2022**, *15*, 877.
- [175] J. Kim, B. S. Kim, A. J. Lee, D. H. Han, J. H. Hwang, Y. Kim, K. C. Song, H. Oh, S. Kim, Y. Park, W. Jeon, *Ceram. Int.* **2022**, *48*, 3236.
- [176] Y. Lee, K. Kim, Z. Lee, H.-S. Lee, H.-B.-R. Lee, W.-H. Kim, I.-K. Oh, H. Kim, *Chem. Mater.* **2023**, 2312.
- [177] M. I. Popovici, A. M. Walke, J. Bizindavyi, J. Meersschaut, K. Banerjee, G. Potoms, K. Katcko, G. Van Den Bosch, R. Delhougne, G. S. Kar, J. Van Houdt, *ACS Appl. Electron. Mater.* **2022**, *4*, 1823.
- [178] K. Yuan, Z. Yu, L. Yang, Y. Yang, J. Sun, *ACS Appl. Nano Mater.* **2022**, *5*, 17949.
- [179] R. Ma, Z. Yu, Z. Ye, Y. Yang, J. Sun, *Appl. Surf. Sci.* **2023**, *639*, 158187.
- [180] A. Tamm, J. Kozlova, L. Aarik, J. Aarik, K. Kukli, J. Link, R. Stern, J. Vac. Sci. Technol. Vac. Surf. Films **2015**, *33*, 01A127.
- [181] P.-A. Hansen, H. Fjellvåg, T. G. Finstad, O. Nilsen, *J. Vac. Sci. Technol. Vac. Surf. Films* **2015**, *34*, 01A130.
- [182] H. Kim, Y. Park, D. Jeong, S. Hong, *Coatings* **2023**, *13*, 491.
- [183] M. D. McDaniel, A. Posadas, T. Q. Ngo, C. M. Karako, J. Bruley, M. M. Frank, V. Narayanan, A. A. Demkov, J. G. Ekerdt, *J. Appl. Phys.* **2014**, *115*, 224108.
- [184] J. Rosa, J. Deuermeier, P. J. Soininen, M. Bosund, Z. Zhu, E. Fortunato, R. Martins, M. Sugiyama, S. Merdes, *Materials* **2020**, *13*, 93.
- [185] Z. Ma, Z. Yu, Y. Yang, J. Sun, *J. Lumin.* **2022**, *241*, 118544.
- [186] Z. Yu, Y. Yang, J. Sun, *Opt. Mater.* **2021**, *122*, 111691.
- [187] Y. Zhang, S. Hu, P. Y. Chen, J. Zhu, B. Chen, R. Bai, H. Zhu, L. Chen, D. W. Zhang, J. C. Lee, Q. Sun, J. G. Ekerdt, L. Ji, *Nanoscale* **2023**, *15*, 9432.
- [188] H. Seim, M. Nieminen, L. Niinistö, H. Fjellvåg, L. S. Johansson, *Appl. Surf. Sci.* **1997**, *112*, 243.
- [189] E. P. Gusev, E. Cartier, D. A. Buchanan, M. Gribelyuk, M. Copel, H. Okorn-Schmidt, C. D'Emic, *Microelectron. Eng.* **2001**, *59*, 341.
- [190] P. A. Hansen, H. Fjellvåg, T. Finstad, O. Nilsen, *Dalton Trans.* **2013**, *42*, 10778.
- [191] E. Atosuo, J. Ojala, M. J. Heikkilä, M. Mattinen, K. Mizohata, J. Räisänen, M. Leskelä, M. Ritala, *J Vac Sci Technol A* **2021**, *39*, 022404.
- [192] P. Myllymäki, M. Nieminen, J. Niinistö, M. Putkonen, K. Kukli, L. Niinistö, *J. Mater. Chem.* **2006**, *16*, 563.
- [193] A. Lamperti, E. Cianci, U. Russo, S. Spiga, O. Salicio, G. Congedo, M. Fanciulli, *J. Vac. Sci. Technol., B: Nanotechnol. Microelectron.: Mater., Process., Meas., Phenom.* **2011**, *29*, 01AE03.
- [194] L. Nyns, J. G. Lisoni, G. Van Den Bosch, S. Van Elshocht, J. Van Houdt, *Phys. Status Solidi Appl. Mater. Sci.* **2014**, *211*, 409.
- [195] H. H. Sønsteby, E. Skaar, Ø. S. Fjellvåg, J. E. Bratvold, H. Fjellvåg, O. Nilsen, *Nat. Commun.* **2020**, *11*, 2872.
- [196] O. Nilsen, M. Peussa, H. Fjellvåg, L. Niinistö, A. Kjekshus, *J. Mater. Chem.* **1999**, *9*, 1781.
- [197] M. Nieminen, S. Lehto, L. Niinistö, *J. Mater. Chem.* **2001**, *11*, 3148.
- [198] K. Bergum, A. Magrasó, H. Fjellvåg, O. Nilsen, *J. Mater. Chem. A* **2014**, *2*, 18463.
- [199] O. Nilsen, E. Rauwel, H. Fjellvåg, A. Kjekshus, *J. Mater. Chem.* **2007**, *17*, 1466.
- [200] M. Lie, O. Nilsen, H. Fjellvåg, A. Kjekshus, *Dalton Trans.* **2009**, 481.
- [201] H. H. Sønsteby, T. Aarholt, Ø. Prytz, H. Fjellvåg, O. Nilsen, *Chem. Commun.* **2018**, *54*, 8253.
- [202] M. Duparc, H. H. Sønsteby, O. Nilsen, A. O. Sjåstad, H. Fjellvåg, *Materials* **2020**, *13*, 24.
- [203] E. Kazyak, K. H. Chen, K. N. Wood, A. L. Davis, T. Thompson, A. R. Bielinski, A. J. Sanchez, X. Wang, C. Wang, J. Sakamoto, N. P. Dasgupta, *Chem. Mater.* **2017**, *29*, 3785.
- [204] T. Aaltonen, M. Alnes, O. Nilsen, L. Costelle, H. Fjellvåg, *J. Mater. Chem.* **2010**, *20*, 2877.
- [205] H. H. Sønsteby, E. Skaar, J. E. Bratvold, J. W. Freeland, A. Yanguas-Gil, J. W. Elam, O. Nilsen, H. Fjellvåg, *J. Mater. Chem. C* **2020**, *8*, 12662.
- [206] T. T. Van, J. P. Chang, *Surf. Sci.* **2005**, *596*, 1.
- [207] N. A. Stafford, R. Katamreddy, L. Guerin, B. Feist, C. Dussarrat, V. Pallem, C. Weiland, R. Opila, *ECS Trans.* **2009**, *19*, 525.
- [208] M. Ameen, L. Nyns, S. Sioncke, D. Lin, T. s. Ivanov, T. Conard, J. Meersschaut, M. Y. Feteha, S. Van Elshocht, A. Delabie, *ECS J. Solid State Sci. Technol.* **2014**, *3*, N133.
- [209] J. H. Han, L. Nyns, A. Delabie, A. Franquet, S. Van Elshocht, C. Adelmann, *Chem. Mater.* **2014**, *26*, 1404.
- [210] M. S. Lebedev, V. N. Kruchinin, M. Y. Afonin, I. V. Korolkov, A. A. Sarayev, A. A. Gismatulin, V. A. Gritsenko, *Appl. Surf. Sci.* **2019**, *478*, 690.
- [211] R. Rahman, J. P. Klesko, A. Dangerfield, M. Fang, J.-S. M. Lehn, C. L. Dezelah, R. K. Kanjolia, Y. J. Chabal, *J Vac Sci Technol A* **2019**, *37*, 011504.
- [212] M. Putkonen, T. Sajavaara, L. S. Johansson, L. Niinistö, *Chem. Vap. Depos.* **2001**, *7*, 44.
- [213] M. Håkansson, M. Helin, M. Putkonen, Q. Jiang, M. Kotiranta, J. Suomi, A. J. Niskanen, T. Ala-Kleme, S. Kulmala, *Anal. Chim. Acta* **2005**, *541*, 135.
- [214] Y. Yang, H. Pei, Z. Ye, J. Sun, *Nanomater* **2023**, *13*, 849.
- [215] J. Niinistö, M. Putkonen, L. Niinistö, *Chem. Mater.* **2004**, *16*, 2953.
- [216] P. Majumder, G. Jursich, A. Kueltzo, C. Takoudis, *J. Electrochem. Soc.* **2008**, *155*, G152.
- [217] C. Dussarrat, N. Blasco, W. Noh, J. Lee, J. Greer, T. Teramoto, S. Kamimura, N. Gosset, T. Ono, *Coatings* **2021**, *11*, 497.
- [218] A. I. Abdulagatov, R. R. Amashaev, K. N. Ashurbekova, S. M. Ramazanov, D. K. Palchaev, A. M. Maksumova, M. K. Rabadanov, I. M. Abdulagatov, *Russ. Microelectron.* **2019**, *48*, 1.
- [219] A. Nishida, T. Katayama, Y. Matsuo, *RSC Adv.* **2023**, *13*, 27255.

- [220] K. Uusi-Esko, J. Malm, M. Karppinen, *Chem. Mater.* **2009**, *21*, 5691.
- [221] K. Uusi-Esko, M. Karppinen, *Chem. Mater.* **2011**, *23*, 1835.
- [222] J. H. Choi, C. Pham, J. Dorman, T. Kim, J. P. Chang, *J. Magn. Magn. Mater.* **2020**, *498*, 166146.
- [223] L. B. Young, C.-K. Cheng, G.-J. Lu, K.-Y. Lin, Y.-H. Lin, H.-W. Wan, M.-Y. Li, R.-F. Cai, S.-C. Lo, C.-H. Hsu, J. Kwo, M. Hong, *J. Vac. Sci. Technol. Vac. Surf. Films* **2017**, *35*, 01B123.
- [224] R. Haugsrud, A. E. Gunnaes, O. Nilsen, *Oxid. Met.* **2003**, *59*, 215.
- [225] X. L. Li, D. Tsoutsou, G. Scarel, C. Wiemer, S. C. Capelli, S. N. Volkos, L. Lamagna, M. Fanciulli, *J. Vac. Sci. Technol. Vac. Surf. Films* **2009**, *27*, L1.
- [226] S. Ahn, P. Littlewood, Y. Liu, T. J. Marks, P. C. Stair, *ACS Catal.* **2022**, *12*, 10522.
- [227] S. J. Jo, J. S. Ha, N. K. Park, D. K. Kang, B. H. Kim, *Thin Solid Films* **2006**, *513*, 253.
- [228] W. Zhao, J. Jiang, Y. Luo, J. Li, Y. Ding, *Coat* **2023**, *13*, 870.
- [229] W. He, D. S. H. Chan, S.-J. Kim, Y.-S. Kim, S.-T. Kim, B. J. Cho, *J. Electrochem. Soc.* **2008**, *155*, G189.
- [230] W. H. Kim, W. J. Maeng, K. J. Moon, J. M. Myoung, H. Kim, *Thin Solid Films* **2010**, *519*, 362.
- [231] T. Suzuki, M. Kouda, P. Ahmet, H. Iwai, K. Kakushima, T. Yasuda, *J. Vac. Sci. Technol. Vac. Surf. Films* **2012**, *30*, 051507.
- [232] B. A. Sperling, J. E. Maslar, S. V. Ivanov, *J. Vac. Sci. Technol. Vac. Surf. Films* **2018**, *36*, 031513.
- [233] S. Kamiyama, E. Kurosawa, Y. Nara, *J. Electrochem. Soc.* **2008**, *155*, H373.
- [234] W. S. Kim, S. K. Park, D. Y. Moon, T. S. Kim, B. W. Kang, J. K. Seo, H. D. Kim, J. W. Park, *J Korean Phys Soc* **2008**, *53*, 3334.
- [235] W. S. Kim, S. K. Park, D. Y. Moon, B. W. Kang, H. D. Kim, J. W. Park, *J Korean Phys Soc* **2009**, *55*, 590.
- [236] H. Kim, S. Woo, J. Lee, H. Kim, Y. Kim, H. Lee, H. Jeon, *J. Electrochem. Soc.* **2010**, *157*, H479.
- [237] Y. Kim, S. Woo, H. Kim, J. Lee, H. Kim, H. Lee, H. Jeona, *J. Mater. Res.* **2010**, *25*, 1898.
- [238] S. R. Patil, V. Y. Borokar, M. Rasadujjaman, J. Zhang, S. J. Ding, A. M. Mahajan, *J Mater Sci Mater Electron* **2023**, *34*, 1284.
- [239] G. Scarel, A. Debernardi, D. Tsoutsou, S. Spiga, S. C. Capelli, L. Lamagna, S. N. Volkos, M. Alia, M. Fanciulli, *Appl. Phys. Lett.* **2007**, *91*, 102901.
- [240] D. Tsoutsou, G. Scarel, A. Debernardi, S. C. Capelli, S. N. Volkos, L. Lamagna, S. Schamm, P. E. Coulon, M. Fanciulli, *Microelectron. Eng.* **2008**, *85*, 2411.
- [241] K. S. Agrawal, V. N. Barhate, V. S. Patil, L. S. Patil, A. M. Mahajan, *Appl. Phys. A: Mater. Sci. Process.* **2020**, *126*, 650.
- [242] W. He, S. Schuetz, R. Solanki, J. Belot, J. McAndrew, *Electrochem. Solid-State Lett.* **2004**, *7*, G131.
- [243] D. H. Triyoso, R. I. Hegde, J. Grant, P. Fejes, R. Liu, D. Roan, M. Ramon, D. Werho, R. Rai, L. B. La, J. Baker, C. Garza, T. Guenther, B. E. White, P. J. Tobin, *J. Vac. Sci. Technol. B Microelectron. Nanometer Struct.* **2004**, *22*, 2121.
- [244] K. Kukli, M. Ritala, V. Pore, M. Leskelä, T. Sajavaara, R. I. Hegde, D. C. Gilmer, P. J. Tobin, A. C. Jones, H. C. Aspinall, *Chem. Vap. Depos.* **2006**, *12*, 158.
- [245] R. Inman, S. A. Schuetz, C. M. Silvernail, S. Balaz, P. A. Dowben, G. Jursich, J. McAndrew, J. A. Belot, *Mater. Chem. Phys.* **2007**, *104*, 220.
- [246] S. Abermann, C. Henkel, O. Bethge, G. Pozzovivo, P. Klang, E. Bertagnolli, *Appl. Surf. Sci.* **2010**, *256*, 5031.
- [247] M. Nieminen, T. Sajavaara, E. Rauhala, M. Putkonen, L. Niinistö, *J. Mater. Chem.* **2001**, *11*, 2341.
- [248] S. Y. Kim, H. Kwon, S. J. Jo, J. S. Ha, W. T. Park, D. K. Kang, B. H. Kim, *Appl. Phys. Lett.* **2007**, *90*, 103104.
- [249] H. H. Sønsteby, E. Østreng, H. Fjellvåg, O. Nilsen, *Thin Solid Films* **2014**, *550*, 90.
- [250] B. S. Lim, A. Rahtu, P. De Rouffignac, R. G. Gordon, *Appl. Phys. Lett.* **2004**, *84*, 3957.
- [251] Y. Liu, H. Kim, J.-J. Wang, H. Li, R. G. Gordon, *ECS Trans.* **2008**, *16*, 471.
- [252] N. M. Sbrockey, M. Luong, E. M. Gallo, J. D. Sloppy, G. Chen, C. R. Winkler, S. H. Johnson, M. L. Taheri, G. S. Tompa, J. E. Spanier, *J. Electron. Mater.* **2012**, *41*, 819.
- [253] C. Fei, H. Liu, X. Wang, X. Fan, *Nanoscale Res. Lett.* **2015**, *10*, 180.
- [254] H. H. Sønsteby, E. Skaar, H. Fjellvåg, O. Nilsen, *ACS Appl. Electron. Mater.* **2021**, *3*, 292.
- [255] A. Del Vitto, R. Piagge, E. Ravizza, S. Spadoni, A. Sebastiani, C. Scozzari, C. Wiemer, G. Chidini, M. Alessandri, M. Fanciulli, J. W. Maes, M. Verghese, *ECS Trans.* **2010**, *33*, 417.
- [256] M. Putkonen, T. Altonen, M. Alnes, T. Sajavaara, O. Nilsen, H. Fjellvåg, *J. Mater. Chem.* **2009**, *19*, 8767.
- [257] H. H. Sønsteby, E. Østreng, O. Nilsen, *Chem. Vap. Depos.* **2014**, *20*, 269.
- [258] H. H. Sønsteby, J. E. Bratvold, K. Weibye, H. Fjellvåg, O. Nilsen, *Chem. Mater.* **2018**, *30*, 1095.
- [259] K. Shen, J. Chang, R. K. Rai, C. Y. Wang, E. A. Stach, R. J. Gorte, J. M. Vohs, *J. Phys. Chem. C* **2023**, *127*, 15591.
- [260] J. M. Gaskell, A. C. Jones, H. C. Aspinall, S. Taylor, P. Taechakumput, P. R. Chalker, P. N. Heys, R. Odedra, *Appl. Phys. Lett.* **2007**, *91*, 112912.
- [261] D. Tsoutsou, L. Lamagna, S. N. Volkos, A. Molle, S. Baldovino, S. Schamm, P. E. Coulon, M. Fanciulli, *Appl. Phys. Lett.* **2009**, *94*, 053504.
- [262] K. B. Jinesh, W. F. A. Besling, E. Tois, J. H. Klootwijk, R. Wolters, W. Dekkers, M. Kaiser, F. Bakker, M. Tuominen, F. Roozeboom, *Appl. Phys. Lett.* **2008**, *93*, 062903.
- [263] S. Abermann, C. Henkel, O. Bethge, E. Bertagnolli, *ECS Meet. Abstr.* **2008**, *MA2008-02*, 1944.
- [264] M. Putkonen, A. Szeghalmi, E. Pippel, M. Knez, *J. Mater. Chem.* **2011**, *21*, 14461.
- [265] J. Päävääri, M. Putkonen, L. Niinistö, *J. Mater. Chem.* **2002**, *12*, 1828.
- [266] P. Cop, E. Celik, K. Hess, Y. Moryson, P. Klement, M. T. Elm, B. M. Smarsly, *ACS Appl. Nano Mater.* **2020**, *3*, 10757.
- [267] D. H. K. Jackson, M. M. Schwartz, C. Ngo, D. Facteau, S. Pylypenko, C. L. Marshall, A. A. Dameron, *J Vac Sci Technol A* **2019**, *37*, 020919.
- [268] H. Hemmelmann, R. Ruess, P. Klement, J. Schörmann, S. Chatterjee, J. Sann, M. T. Elm, *Adv. Mater. Interfaces* **2023**, *10*, 2202268.
- [269] W.-H. Kim, M.-K. Kim, W. J. Maeng, J. Gatineau, V. Pallem, C. Dussarrat, A. Noori, D. Thompson, S. Chu, H. Kim, *J. Electrochem. Soc.* **2011**, *158*, G169.
- [270] W. J. Maeng, I. K. Oh, W. H. Kim, M. K. Kim, C. W. Lee, C. Lansalot-Matas, D. Thompson, S. Chu, H. Kim, *Appl. Surf. Sci.* **2014**, *321*, 214.
- [271] U. Kumar, C. Feit, S. N. Berriel, A. Arunachalam, T. S. Sakthivel, K. Basu, P. Banerjee, S. Seal, *J Vac Sci Technol A* **2021**, *39*, 060405.
- [272] E. Gourba, A. Ringuedé, M. Cassir, A. Billard, J. Päävääri, J. Niinistö, M. Putkonen, L. Niinistö, *Ionics* **2003**, *9*, 15.
- [273] K. Shen, S. Lee, O. Kwon, M. Fan, R. J. Gorte, J. M. Vohs, *ACS Catal.* **2023**, *13*, 11144.
- [274] K. Shen, M. Fan, R. K. Rai, E. A. Stach, R. J. Gorte, J. M. Vohs, *J. Solid State Chem.* **2023**, *323*, 124055.
- [275] H. Kondo, H. Matsui, K. Furuta, M. Sakashita, S. Zaima, *Jpn. J. Appl. Phys.* **2010**, *49*, 04DA14.
- [276] J. M. Gaskell, S. Przybylak, A. C. Jones, H. C. Aspinall, P. R. Chalker, K. Black, R. J. Potter, P. Taechakumput, S. Taylor, *Chem. Mater.* **2007**, *19*, 4796.

- [277] W. L. I. Waduge, Y. Chen, P. Zuo, N. Jayakodiarachchi, T. F. Kuech, S. E. Babcock, P. G. Evans, C. H. Winter, *ACS Appl. Nano Mater.* **2019**, 2, 7449.
- [278] L. Khomenkova, H. Merabet, M. P. Chauvat, C. Frilay, X. Portier, C. Labbe, P. Marie, J. Cardin, S. Boudin, J. M. Rueff, F. Gourbilleau, *Surf. Interfaces* **2022**, 34, 102377.
- [279] Y. Sun, Q. Wang, T. J. Park, T. E. Gage, Z. Zhang, X. Wang, D. Zhang, X. Sun, J. He, H. Zhou, D. G. Lim, C. Huang, H. Yu, X. Chen, H. Wang, J. Mei, E. Deguns, S. Ramanathan, *ACS Appl. Electron. Mater.* **2021**, 3, 1719.
- [280] E. Rauwel, A. Galeckas, P. Rauwel, P. A. Hansen, D. Wragg, O. Nilsen, H. Fjellvåg, *Mater. Res. Express* **2016**, 3, 055010.
- [281] E. Rauwel, A. Galeckas, P. Rauwel, P.-A. Hansen, D. Wragg, O. Nilsen, H. Fjellvåg, *ECS Meet. Abstr.* **2014**, MA2014-02, 1599.
- [282] P. A. Hansen, C. S. Granerød, Ø. Prytz, O. Nilsen, *J. Lumin.* **2019**, 215, 116618.
- [283] P. A. Hansen, T. G. Finstad, O. Nilsen, *Chem. Vap. Depos.* **2014**, 20, 274.
- [284] A. Ferrier, N. Harada, M. Scarafaglio, E. Briand, J. J. Ganem, I. Vickridge, A. Seyeux, P. Marcus, D. Serrano, P. Goldner, A. Tallaire, *J. Phys. Chem. C* **2020**, 124, 19725.
- [285] P. A. Hansen, H. Fjellvåg, T. G. Finstad, O. Nilsen, *RSC Adv.* **2014**, 4, 11876.
- [286] M. N. Getz, P. A. Hansen, H. Fjellvåg, O. Nilsen, *RSC Adv.* **2017**, 7, 8051.
- [287] H. Kim, H. J. Yun, B. J. Choi, *RSC Adv.* **2018**, 8, 42390.
- [288] H. J. Yun, S. Y. Ryu, H. Y. Lee, W. Y. Park, S. G. Kim, B. J. Choi, *Ceram. Int.* **2021**, 47, 16597.
- [289] A. P. Milanov, R. A. Fischer, A. Devi, *Inorg. Chem.* **2008**, 47, 11405.
- [290] R. Ranjith, A. Laha, E. Bugiel, H. J. Osten, K. Xu, A. P. Milanov, A. Devi, *Semicond. Sci. Technol.* **2010**, 25, 105001.
- [291] S. Dueñas, H. Castán, H. García, A. Gómez, L. Bailón, K. Kukli, T. Hatanpää, J. Lu, M. Ritala, M. Leskelä, *J. Electrochem. Soc.* **2007**, 154, G207.
- [292] H. García, S. Dueñas, H. Castán, A. Gómez, L. Bailón, R. Barquero, K. Kukli, M. Ritala, M. Leskelä, *J. Vac. Sci. Technol. B Microelectron. Nanometer Struct.* **2009**, 27, 416.
- [293] S. A. Vitale, P. W. Wyatt, C. J. Hodson, *J. Vac. Sci. Technol. Vac. Surf. Films* **2012**, 30, 01A130.
- [294] J. H. Han, A. Delabie, A. Franquet, T. Conard, S. Van Elshocht, C. Adelmann, *Chem. Vap. Depos.* **2015**, 21, 352.
- [295] C. Adelmann, D. Pierreux, J. Swerts, D. Dewulf, A. Hardy, H. Tielens, A. Franquet, B. Brijs, A. Moussa, T. Conard, M. K. Van Bael, J. W. Maes, M. Jurczak, J. A. Kittl, S. Van Elshocht, *Chem. Vap. Depos.* **2010**, 16, 170.
- [296] I. Jögi, A. Tamm, K. Kukli, M. Kemell, J. Lu, T. Sajavaara, M. Ritala, M. Leskelä, *J. Electrochem. Soc.* **2010**, 157, G202.
- [297] P. Myllymäki, M. Roeckerath, M. Putkonen, S. Lenk, J. Schubert, L. Niinistö, S. Mantl, *Appl. Phys. A: Mater. Sci. Process.* **2007**, 88, 633.
- [298] C. Bohr, P. Yu, M. Scigaj, C. Hegemann, T. Fischer, M. Coll, S. Mathur, *Thin Solid Films* **2020**, 698, 137848.
- [299] Y. Yang, N. Li, J. Sun, *Opt. Express* **2018**, 26, 9344.
- [300] E. Cianci, A. Lamperti, G. Congedo, S. Spiga, *ECS J. Solid State Sci. Technol.* **2012**, 1, P5.
- [301] I. K. Oh, K. Kim, Z. Lee, K. Y. Ko, C. W. Lee, S. J. Lee, J. M. Myung, C. Lansalot-Matras, W. Noh, C. Dussarrat, H. Kim, H. B. R. Lee, *Chem. Mater.* **2015**, 27, 148.
- [302] T. T. Van, J. P. Chang, *Appl. Surf. Sci.* **2005**, 246, 250.
- [303] R. Xu, C. G. Takoudis, *ECS J. Solid State Sci. Technol.* **2012**, 1, N107.
- [304] C. L. Dezelah, P. Myllymäki, J. Päiväsari, K. Arstila, L. Niinistö, C. H. Winter, *J. Mater. Chem.* **2007**, 17, 1308.
- [305] S. Vangelista, A. Lamperti, C. Wiemer, M. Fanciulli, R. Mantovan, *Thin Solid Films* **2016**, 604, 18.
- [306] Y. Liu, Z. Ouyang, J. Liu, L. Yang, Y. Yang, J. Sun, *J. Phys. Appl. Phys.* **2020**, 53, 215104.
- [307] Y. Liu, Z. Ouyang, L. Yang, Y. Yang, J. Sun, *Nanomaterials* **2019**, 9, 413.
- [308] R. E. Agbenyeke, E. A. Jung, B. K. Park, T. M. Chung, C. G. Kim, J. H. Han, *Appl. Surf. Sci.* **2017**, 419, 758.
- [309] M. Bosund, K. Mizohata, T. Hakkarainen, M. Putkonen, M. Söderlund, S. Honkanen, H. Lipsanen, *Appl. Surf. Sci.* **2009**, 256, 847.
- [310] M. Getz, P. A. Hansen, M. A. K. Ahmed, H. Fjellvåg, O. Nilsen, *Dalton Trans.* **2017**, 46, 3008.
- [311] G. Scarel, E. Bonera, C. Wiemer, G. Tallarida, S. Spiga, M. Fanciulli, I. L. Fedushkin, H. Schumann, Y. u. Lebedinskii, A. Zenkevich, *Appl. Phys. Lett.* **2004**, 85, 630.
- [312] E. Bonera, G. Scarel, M. Fanciulli, P. Delugas, V. Fiorentini, *Phys. Rev. Lett.* **2005**, 94, 027602.
- [313] C. Adelmann, J. Swerts, T. Conard, B. Brijs, A. Franquet, A. Hardy, H. Tielens, K. Opsomer, A. Moussa, M. K. Van Bael, M. Jurczak, J. A. Kittl, S. Van Elshocht, *ECS Trans.* **2011**, 34, 473.
- [314] J. L. T. M. Moret, M. B. E. Griffiths, J. E. B. M. Frijns, B. E. Terpstra, H. T. Wolterbeek, S. T. Barry, A. G. Denkova, J. R. van Ommen, *J Vac Sci Technol A* **2020**, 38, 022414.
- [315] G. Scarel, C. Wiemer, G. Tallarida, S. Spiga, G. Seguini, E. Bonera, M. Fanciulli, Y. Lebedinskii, A. Zenkevich, G. Pavia, I. L. Fedushkin, G. K. Fukin, G. A. Domrachev, *J. Electrochem. Soc.* **2006**, 153, F271.
- [316] Z. Ma, Z. Yu, X. Guo, Y. Yang, J. Sun, *ACS Appl. Nano Mater.* **2023**, 6, 12312.
- [317] Z. Giedraityte, L. S. Johansson, M. Karppinen, *RSC Adv.* **2016**, 6, 103412.
- [318] A. Ghazy, M. Lastusaari, M. Karppinen, *Chem. Mater.* **2023**, 35, 5988.
- [319] M. Safdar, A. Ghazy, M. Tuomisto, M. Lastusaari, M. Karppinen, *J. Mater. Sci.* **2021**, 56, 12634.
- [320] A. Ghazy, M. Lastusaari, M. Karppinen, *J. Mater. Chem. C* **2023**, 11, 5331.
- [321] Z. Giedraityte, M. Tuomisto, M. Lastusaari, M. Karppinen, *ACS Appl. Mater. Interfaces* **2018**, 10, 8845.
- [322] M. Tuomisto, Z. Giedraityte, L. Mai, A. Devi, V. Boiko, K. Grzeszkiewicz, D. Hreniak, M. Karppinen, M. Lastusaari, *J. Lumin.* **2019**, 213, 310.
- [323] Y. Yang, L. Chen, F. Jiang, M. Yu, X. Wan, B. Zhang, M. Hong, *J. Mater. Chem. C* **2017**, 5, 1981.
- [324] A. De Bettencourt-Dias, *Luminescence of Lanthanide Ions in Coordination Compounds and Nanomaterials*, John Wiley & Sons Ltd, Chichester, United Kingdom, 2014.
- [325] J. Penttilä, M. Nisula, M. Karppinen, *Chemistry* **2017**, 23, 18225.
- [326] A. Ghazy, M. Safdar, M. Lastusaari, M. Karppinen, *Chem. Commun.* **2020**, 56, 241.
- [327] P. A. Hansen, J. Svendsen, H. Nesteng, O. Nilsen, *RSC Adv.* **2022**, 12, 18063.
- [328] R. M. Silva, L. D. Carlos, J. Rocha, R. F. Silva, *Appl. Surf. Sci.* **2020**, 527, 146603.
- [329] K. H. Goh, A. S. M. A. Haseeb, Y. H. Wong, *Mater. Sci. Semicond. Process.* **2017**, 68, 302.
- [330] J. Robertson, R. M. Wallace, *Mater Sci Eng R Rep* **2015**, 88, 1.
- [331] J. Robertson, *J Vac Sci Technol B Microelectron Nanometer Struct Process Meas Phenom* **2000**, 18, 1785.
- [332] L. Yang, J. Luo, L. Gao, B. Song, J. Tang, *J. Phys. Chem. Lett.* **2022**, 2022, 4365.
- [333] T. Harazono, R. Adachi, Y. Shimomura, T. Watanabe, *Phys. Chem. Chem. Phys.* **2001**, 3, 2943.
- [334] M. Bieza, M. Guzik, E. Tomaszewicz, Y. Guyot, K. Lebbou, G. Boulon, *J. Phys. Chem. C* **2017**, 121, 13303.

- [335] J. D. B. Bradley, M. Pollnau, *Laser Photonics Rev.* **2011**, *5*, 368.
- [336] M. Pan, W. M. Liao, S. Y. Yin, S. S. Sun, C. Y. Su, *Chem. Rev.* **2018**, *118*, 8889.
- [337] S. SeethaLekshmi, A. R. Ramya, M. L. P. Reddy, S. Varughese, *J. Photochem. Photobiol. C Photochem. Rev.* **2017**, *33*, 109.
- [338] A. R. Ramya, S. Varughese, M. L. P. Reddy, *Dalton Trans.* **2014**, *43*, 10940.
- [339] Z. Zhang, Y. Chen, H. Chang, Y. Wang, X. Li, X. Zhu, *J. Mater. Chem. C* **2020**, *8*, 2205.
- [340] V. Kumar, V. Bhardwaj, A. Kaushik, *ACS Appl. Electron. Mater.* **2021**, *3*, 2261.
- [341] S. Tabanli, G. Eryurek, *J. Nanophotonics* **2018**, *12*, 026008.
- [342] Y. Zhang, J. Hao, *J. Appl. Phys.* **2013**, *113*, 184112.
- [343] A. Nadort, J. Zhao, E. M. Goldys, *Nanoscale* **2016**, *8*, 13099.
- [344] J. Benick, B. Hoex, M. C. M. Van De Sanden, W. M. M. Kessels, O. Schultz, S. W. Glunz, *Appl. Phys. Lett.* **2008**, *92*, 253504.
- [345] G. Chen, J. Shen, T. Y. Ohulchanskyy, N. J. Patel, A. Kutikov, Z. Li, J. Song, R. K. Pandey, H. Agren, P. N. Prasad, G. Han, *ACS Nano* **2012**, *6*, 8280.
- [346] M. R. Hamblin, *Dalton Trans.* **2018**, *47*, 8571.
- [347] D. Yang, P. Ma, Z. Hou, Z. Cheng, C. Li, J. Lin, *Chem. Soc. Rev.* **2015**, *44*, 1416.
- [348] W. R. Algar, N. Hildebrandt, S. S. Vogel, I. L. Medintz, *Nat. Methods* **2019**, *16*, 815.
- [349] H. Sahoo, *J. Photochem. Photobiol. C Photochem. Rev.* **2011**, *12*, 20.
- [350] S. Hepojoki, J. Rusanen, J. Hepojoki, V. Nurmi, A. Vaheri, Å. Lundkvist, K. Hedman, O. Vapaalahti, *J Clin Microbiol* **2015**, *53*, 2292.
- [351] I. Hemmilä, V. Laitala, *J Fluoresc* **2005**, *15*, 529.
- [352] M. Weber, N. Boysen, O. Graniel, A. Sekkat, C. Dussarrat, P. Wiff, A. Devi, D. Muñoz-Rojas, *ACS Mater Au* **2023**, *3*, 274.
- [353] J. N. Brönsted, *Recl. Trav. Chim. Pays-Bas* **1923**, *4*, 514.



Amr Ghazy obtained his doctoral degree in 2023 from the School of Chemical Engineering at Aalto University. He carried out his doctoral research in the Inorganic Materials Chemistry research group under the supervision of Prof. Karppinen. The research focus was on novel photoluminescent and upconverting lanthanide-organic thin films fabricated using ALD/MLD and investigated for solar cells, visible-light luminescence, and bioimaging. Recently he was recruited as a Process Development Engineer at Kalpana Systems in Delft, the Netherlands.



David Zanders obtained his binational doctoral degree in chemistry in 2022 from the Ruhr University Bochum (Germany) and Carleton University (Canada). His Ph.D. studies were dedicated to the development of novel precursors, process chemistries, and ALD processes of metallic thin films for interconnect application in microelectronics which was jointly supervised by Prof. A. Devi and Prof. S. T. Barry. In 2023, he joined ASM International's Corporate Research and Development department on the premises of IMEC in Leuven, Belgium aiming to contribute to the development of next-generation semiconductor devices.



Anjana Devi received her Ph.D. in 1998 from the Indian Institute of Science (India). She moved to Germany as an Alexander von Humboldt fellow for postdoctoral research. From 2002 to 2023, she was a Professor of Inorganic Materials Chemistry at the Ruhr University Bochum. Her research focuses on novel precursor chemistries and their applications in ALD and MOCVD of nanostructured thin films. She was conferred the honorary doctorate of Technology from Aalto University in 2020. Since 2021, she has been heading the Nanostructured Sensor Materials Research Group at the Fraunhofer Institute for Microelectronic Circuits and Systems (IMS) in Duisburg. Starting January 2024, she is the Director of the Institute for Materials Chemistry at the Leibniz Institute of Solid State and Materials Research, IFW Dresden and Chair of Materials Chemistry at the Dresden University of Technology (TUD) in Dresden (Germany).



Maarit Karppinen received her Ph.D. in 1993. Before establishing her Inorganic Materials Chemistry group at Aalto University in 2006, she was holding a professor chair at Tokyo Institute of Technology. Her research is focused on new ALD/MLD-enabled functional materials, for which she has received two ERC AdG grants in 2014 and 2023, the first one followed by ERC PoC grants in 2015 (flexible thermoelectrics) and 2017 (Li-organic micro battery). This multidisciplinary research covers the design and synthesis of novel inorganic–organic materials and their characterization for various emerging applications. In 2017 prof. Karppinen was nominated as an Aalto Distinguished Professor and in 2019 a Visiting International Professor at the Ruhr University Bochum, Germany.